NTIA-Report-80-51

Calculation of Geostationary Satellite Footprints for Certain Idealized Antennas

K.P. Spies

E.J. Haakinson

U.S. DEPARTMENT OF COMMERCE
Philip M. Klutznick, Secretary

Henry Geller, Assistant Secretary
for Communications and Information

October 1980

TABLE OF CONTENTS

	Page
LIST OF FIGURES	iv
ABSTRACT	1
1. INTRODUCTION	1
1.1 Purpose	1
1.2 Approximations and Limitations	2
2. FOOTPRINTS FOR AN ARBITRARY ANTENNA BEAM	5
2.1 Introduction	5
2.2 Coordinate Geometry	5
2.3 Calculation of Intersection Points	7
2.4 Limb Line Calculations	13
2.5 Footprint Calculations	15
3. CIRCULAR APERTURE ANTENNAS	19
3.1 Introduction	19
3.2 Radiation Patterns	19
3.3 Footprint Calculations for Circular Aperture Antennas	26
4. ELLIPTICAL APERTURE ANTENNAS	31
4.1 Introduction	31
4.2 Radiation Patterns	34
4.3 A Special Case	36
4.4 Footprint Calculations for Elliptical Aperture Antennas	40
5. RECTANGULAR APERTURE ANTENNAS	42
5.1 Introduction	42
5.2 Radiation Patterns	42
5.3 Some Special Cases	44
5.4 Footprint Calculations for Rectangular Aperture Antennas	47
6. HELICAL BEAM ANTENNAS	50
6.1 Introduction	50
6.2 Radiation Patterns	50
6.3 Footprint Calculations for Helical Beam Antennas	52
7. REFERENCES	53

LIST OF FIGURES

Figure		Page
1-1	Scheme for approximating geostationary satellite antenna footprints. .	4
2-1	Coordinate geometry for intersection calculations.	6
2-2	Geometry for specifying direction of line from satellite	8
2-3	Relation between the unit vectors $\underline{e}_\xi$, $\underline{e}_z$, and $\underline{e}_\eta$	10
2-4	Geometry for limb line calculations.	14
2-5	Footprints illustrating relation between contour shape and optimum arrangement of representative points	17
2-6	Hypothetical footprint reflecting complex side-lobe structure of antenna pattern	18
3-1	Geometry for the circular aperture antenna	20
3-2	Typical aperture amplitude distribution used in FOOTPRINTS program for idealized circular aperture antenna	23
3-3	Typical plot of normalized far-field power density $\hat{P}(\alpha)$ vs. off-axis angle α for an idealized circular aperture antenna	28
3-4	Typical plot of normalized far-field amplitude function $\hat{F}(\alpha)$ vs. off-axis angle α for an idealized circular aperture antenna	29
3-5	Generalized flowchart for an algorithm implementing bisection method of evaluating α_S	32
3-6	Generalized flowchart for an algorithm implementing modified false position method of evaluating α_S	33
4-1	Geometry for the elliptical aperture antenna	35
4-2	Geometry for specifying orientation of elliptical aperture antenna . .	41
5-1	Geometry for the rectangular aperture antenna	43
5-2	Geometry for specifying orientation of rectangular aperture antenna .	48
6-1	Geometry for the helical beam antenna	51

CALCULATION OF GEOSTATIONARY SATELLITE FOOTPRINTS FOR CERTAIN IDEALIZED ANTENNAS

K. P. Spies and E. J. Haakinson*

This report describes methods for calculating, under certain simplifying assumptions, footprints (contours of constant power density) for idealized models of several common types of transmitting antennas (circular aperture, elliptical aperture, rectangular aperture, and helical beam antennas), and for antenna beams of specified but rather arbitrary shape. The transmitter is mounted on a satellite at a prescribed location in the geostationary orbit and has its main-lobe axis directed toward a given aim point on the earth.

Formulas are first derived for calculating the intersection of the earth with a ray emanating from a given geostationary satellite and having a prescribed direction in space. For each idealized antenna type, procedures are next discussed for finding those directions in space where the relative power density has a specified constant value; intersection formulas are then applied to locate the corresponding footprint. Far-field patterns are approximated for aperture antennas by evaluating Fourier transforms of assumed aperture illumination distributions, and for the helix by assuming it radiates in the axial mode. Owing to gross discrepancies between actual and ideal side-lobe patterns, the analysis is confined to the main lobe of idealized antenna models.

Key words: antenna patterns; footprints; geostationary satellite; power density contours

1. INTRODUCTION

1.1 Purpose

Transmitting antennas mounted on satellites and beaming signals toward the earth may, depending on characteristics of the particular antenna, illuminate virtually the entire visible earth with a nearly uniform power density**, or they may concentrate most of their radiation on a rather limited area of the earth's surface. In any event, it is often useful to describe the received fields of a satellite antenna by means of contours of constant power density at the earth's surface. Such contours, commonly called "earth footprints" or simply "footprints," are utilized by communication system designers and spectrum managers in maximizing

*The authors are with the Institute for Telecommunication Sciences, National Telecommunications and Information Administration, U.S. Department of Commerce, Boulder, Colorado 80303

**Everywhere in this report, the term "power density" implies a spatial density; i.e., power/unit area (expressed in mks units as watts per square meter), and should not be confused with power spectral density.

a satellite antenna's coverage of a particular geographic area, and in minimizing the effects of interference on other communication systems.

A desirable engineering aid in the design and development of a satellite antenna system is the ability to plot, on appropriate maps of the earth's surface, footprints corresponding to given levels of power density. To this end, a computer program (FOOTPRINTS) has been written (Haakinson et al., 1977) which automatically calculates and plots footprints for idealized models of several common types of transmitting antennas (circular aperture antennas, elliptical aperture antennas, rectangular aperture antennas, and helical beam antennas) and for antenna beams of specified but rather arbitrary shape, when the transmitter is mounted on a satellite at a prescribed location in the geostationary orbit and has its main-lobe axis directed toward a given point (the "aim point") on the earth. The purpose of this report is to describe computational procedures used by the FOOTPRINTS program in determining contours of constant power density.

1.2 Approximations and Limitations

In applications for which these calculations are intended, it is not necessary to locate footprints with great precision. To facilitate our task, we make two simplifying assumptions. First, we neglect all effects resulting from the interaction of antenna radiation with the earth and its atmosphere (e.g., we ignore diffraction, refraction, scattering, and absorption). Second, for points on the illuminated earth's surface, we neglect the small variations of received power density that are due to slightly differing distances from the transmitter.

Under these assumptions, we then approximate the footprint corresponding to a prescribed relative power density as follows: Suppose the antenna's three-dimensional relative power density pattern to have its origin at the satellite and be oriented with its main-lobe axis directed toward the aim point. Now consider the set of points where the power pattern assumes the prescribed value; these points will, in general, form one or several simple closed curves, which may be regarded as the intersection of the power pattern with a sphere centered at the satellite and having a radius equal to the given power density. A straight line, drawn from the satellite (i.e., the pattern origin) through any such point, corresponds to a direction in space for which the antenna's relative power density has the prescribed value. The set of all such lines forms, in general, one nappe of a cone whose vertex is at the satellite, and whose intersection with the illuminated earth's surface constitutes the desired footprint. This situation is

illustrated in Figure 1-1, where we indicate a footprint for a geostationary satellite antenna located at S with its main-lobe axis directed toward the aim point A on the earth.

The task of determining footprints is further simplified by assuming the earth to be a sphere, rather than any of the various spheroids commonly used in geodesy. Once the shape of the cone (corresponding to a constant relative power density) is specified, the footprint calculations then reduce to finding the intersection of a sphere and a cone.

For the idealized antennas considered in this report, we restrict our attention to main-lobe patterms, which simulate those of actual antennas sufficiently well (from a fraction of a decibel at peaks to within a few decibels near nulls) to be of value in footprint applications. However, these idealized models generally fail to provide a useful approximation to side-lobe patterns of actual antennas, since the latter are strongly dependent upon characteristics of the particular antenna (e.g., primary illumination, spill-over loss, aperture blocking) and upon the geometry of nearby devices on the satellite.

Finally, we mention certain approximations implicit in our assumption that the satellite is in a geostationary orbit about a spherical earth--viz., that the earth rotates at a uniform rate on a fixed axis, that the earth's density distribution is spherically symmetric, and that the effects of atmospheric drag are ignored, as are graviatational perturbations due to the moon and sun. In such an idealized situation, it then follows that the geostationary satellite is located in the earth's equatorial plane and its distance s from the earth's center is given by

$$s = \left(\frac{GMP^2}{4\pi^2}\right)^{\frac{1}{3}} = 6.62\ a \quad , \tag{1-1}$$

where $G = 6.670 \times 10^{-11}$ is the universal gravitation constant (in mks units), $M = 5.976 \times 10^{24}$ kg is the earth's mass, $P = 86{,}164$ sec is the earth's rotation period, and $a = 6371$ km is the earth's mean radius. Thus, the location of an ideal geostationary satellite is completely determined by specifying its longitude (λ_s in Fig. 1-1), or in more precise terms, by specifying the (geographic) longitude of the so-called "sub-satellite point." As indicated in Figure 1-1, the latter is the point (S') on the earth's surface that is directly below the satellite.

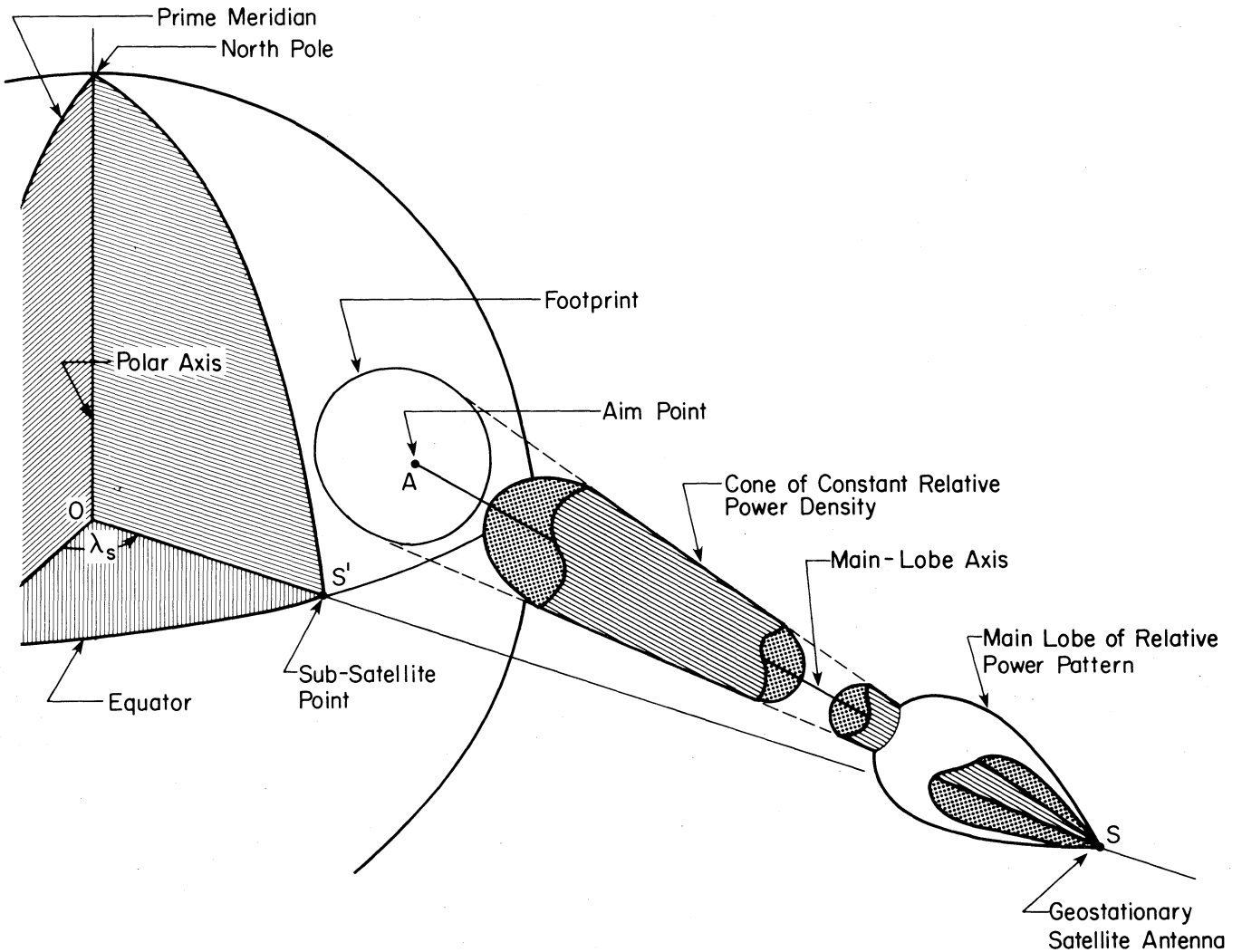

Figure 1-1. Scheme for approximating geostationary satellite antenna footprints.

2. FOOTPRINTS FOR AN ARBITRARY ANTENNA BEAM

2.1 Introduction

In this section, we derive formulas for calculating the latitude and longitude of the intersection of a straight line, emanating from a given geostationary satellite and having a prescribed direction in space, with a spherical earth. By relating an appropriate set of such lines to the main-lobe axis of an antenna on the satellite, our formulas can be used to generate footprints when the cone corresponding to a particular constant relative power density has essentially any specified shape. This capability includes, for example, the generation of rather complex footprints arising from the side lobes of an actual antenna. Our approach is an adaptation and modest extension of that used by Ott (1975) to calculate footprints for antenna beams having elliptical cross-sections.

2.2 Coordinate Geometry

We assume the earth to be a sphere with unit radius centered at the origin 0 of the right-handed system of rectangular coordinates (x,y,z) indicated in Figure 2-1. Note that the earth's polar axis corresponds to the z-axis of the rectangular coordinate system, with the north geographical pole being located at (0,0,1). The earth's equatorial plane then corresponds to the (x,y)-plane, and the intersection of the prime (Greenwich) meridian and the equator is located at (1,0,0). Note also, since the earth is assumed to have a radius of unity, that all distances are expressed in earth radii.

Let the geostationary satellite, located at the fixed point S in the (x,y)-plane, be a distance s = 6.62 from the origin 0 and have a longitude λ_s. If $\underline{s}$ denotes the vector from 0 to S, then in terms of the unit vectors $\underline{e}_x$, $\underline{e}_y$, $\underline{e}_z$ along the positive x-, y-, and z-axes, respectively, we have

$$\underline{s} = s_x \underline{e}_x + s_y \underline{e}_y \quad , \tag{2-1}$$

where

$$s_x = s \cos \lambda_s \text{ and } s_y = s \sin \lambda_s \quad . \tag{2-2}$$

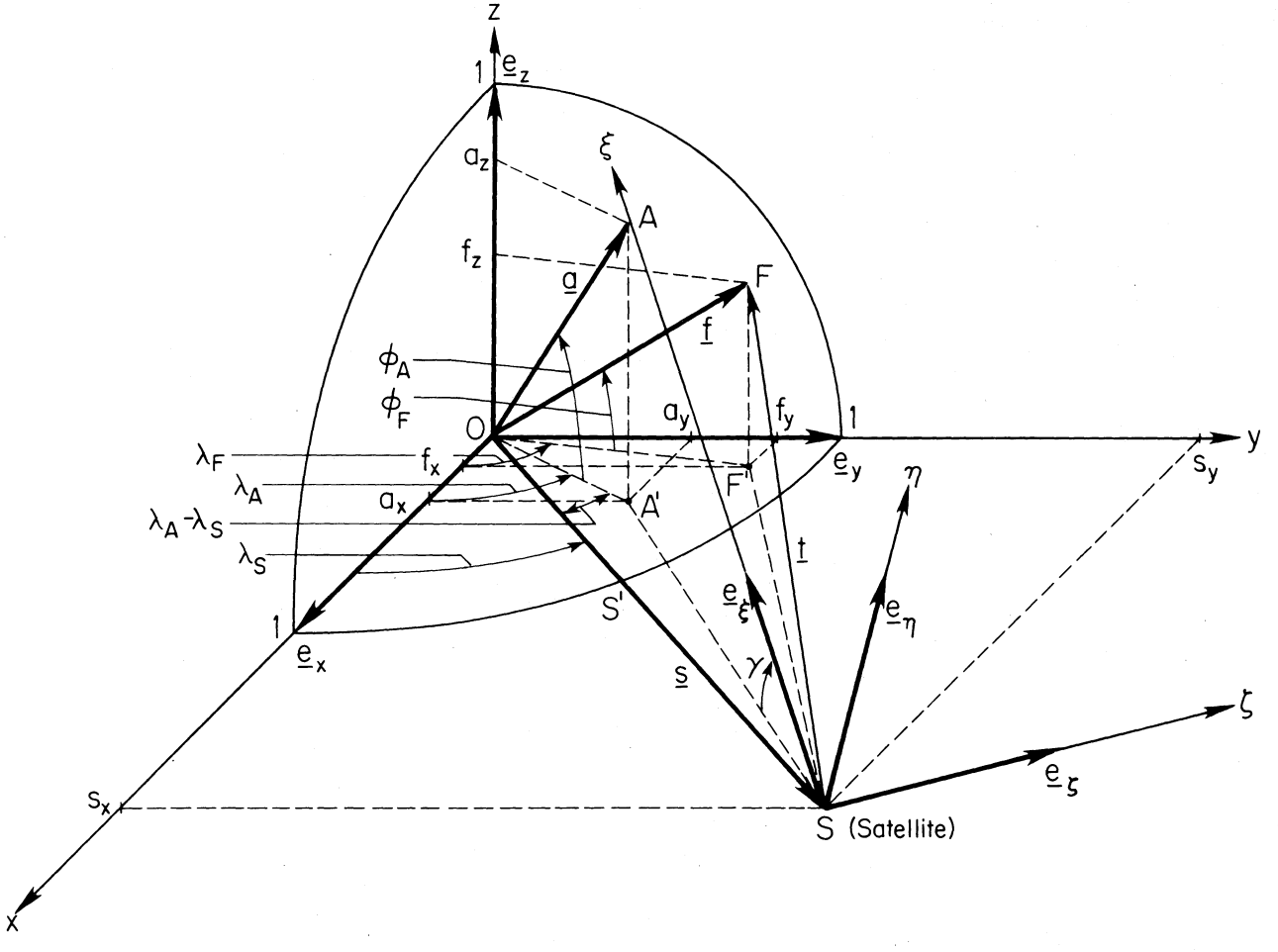

Figure 2-1. Coordinate geometry for intersection calculations.

Let the aim point A have latitude ϕ_A and longitude λ_A; if $\underline{a}$ denotes the (unit) vector from O to A, then

$$\underline{a} = a_x \underline{e}_x + a_y \underline{e}_y + a_z \underline{e}_z \quad , \tag{2-3}$$

where

$$a_x = \cos \phi_A \cos \lambda_A, \quad a_y = \cos \phi_A \sin \lambda_A, \quad a_z = \sin \phi_A \quad . \tag{2-4}$$

A second right-handed system of rectangular coordinates (ξ,η,ζ) has its origin at the satellite S, and is oriented as follows (see Fig. 2-1):

i) the positive ξ-axis is directed from S toward the aim point A (i.e., it lies along the main-lobe axis of the antenna);

ii) the η-axis lies in the plane that is normal to the equator and contains the ξ-axis, positive values of η being located in the $z>0$ half-space; and

iii) the ζ-axis completes the right-handed system so that $\underline{e}_\zeta = \underline{e}_\xi \times \underline{e}_\eta$, where, as usual, we use $\underline{e}_\xi$, $\underline{e}_\eta$, $\underline{e}_\zeta$ to denote unit vectors along the positive ξ-, η-, and ζ-axes, respectively. Note that the ζ-axis lies in the equatorial plane, since it is normal to the (ξ,η)-plane at S and the (ξ,η)-plane is normal to the equator.

2.3 Calculation of Intersection Points

The direction in space of a line from S (i.e., of a typical element of the cone corresponding to some constant relative power density) is now determined by specifying its orientation with respect to the (ξ,η,ζ) coordinate system. In particular, we specify the angles α and ω, where (as indicated in Figure 2-2):

i) α is measured from the positive ξ-axis to the line (i.e., from the antenna's main-lobe axis to the cone element), and

ii) ω is measured from the positive η-axis to the projection of the line in the (η,ζ)-plane, the positive sense of ω being clockwise for an observer looking in the direction of increasing ξ. Note that α and ω correspond to the colatitude and longitude, respectively, in a spherical coordinate system centered at S and having the ξ-axis as its polar axis.

Now suppose that the line from S, characterized by the angles α and ω, intersects the earth at the point F (see Fig. 2-1). We wish to calculate the latitude

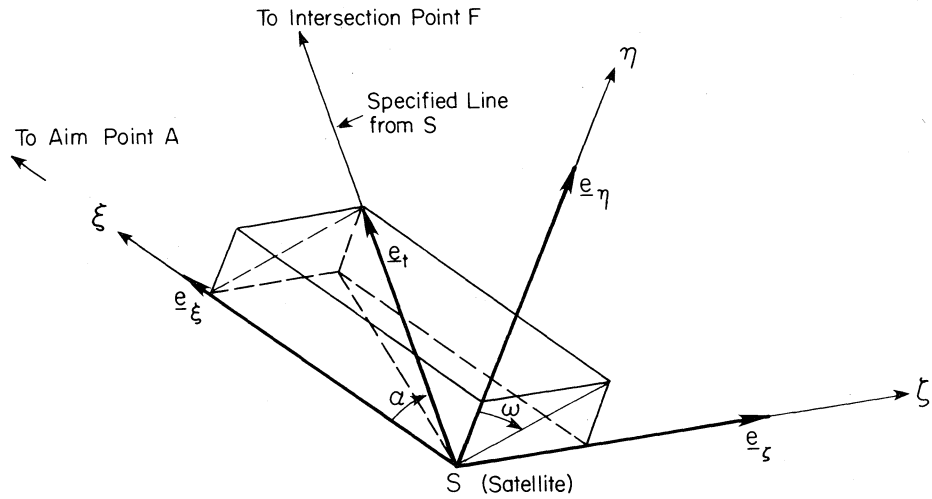

Figure 2-2. Geometry for specifying direction of line from satellite.

ϕ_F and longitude λ_F of F in terms of the satellite distance s and longitude λ_S, the aim point coordinates ϕ_A and λ_A. and the angles α and ω. Let

$$\underline{f} = f_x \underline{e}_x + f_y \underline{e}_y + f_z \underline{e}_z \tag{2-5}$$

be the (unit) vector from 0 to F, and

$$\underline{t} = t_x \underline{e}_x + t_y \underline{e}_y + t_z \underline{e}_z \tag{2-6}$$

be the vector from S to F, then note that

$$\underline{f} = \underline{s} + \underline{t} \quad . \tag{2-7}$$

Now, the <u>direction</u> of $\underline{t}$ is known; from Figure 2-2, a unit vector $\underline{e}_t$ in the direction of $\underline{t}$ can be written as

$$\underline{e}_t = (\cos\alpha)\, \underline{e}_\xi + (\sin\alpha \cos\omega)\, \underline{e}_\eta + (\sin\alpha \sin\omega)\, \underline{e}_\zeta \quad . \tag{2-8}$$

If we let t denote the (as yet unknown) magnitude of $\underline{t}$, so that $\underline{t} = t\, \underline{e}_t$, then we can also write

$$\underline{e}_t = (t_x/t)\, \underline{e}_x + (t_y/t)\, \underline{e}_y + (t_z/t)\, \underline{e}_z \quad . \tag{2-9}$$

The components t_x/t, t_y/t, t_z/t of $\underline{e}_t$ can be found by replacing each of the unit vectors $\underline{e}_\xi$, $\underline{e}_\eta$, $\underline{e}_\zeta$ in (2-8) by the appropriate linear combination of the unit vectors $\underline{e}_x$, $\underline{e}_y$, $\underline{e}_z$, then equating the resulting expression for $\underline{e}_t$ to the right side of (2-9).

We start with $\underline{e}_\xi$; if d_1 denotes the (known) distance from S to A, then the vector from S to A can be written as $d_1\,\underline{e}_\xi$. From the relation

$$\underline{s} + d_1\,\underline{e}_\xi = \underline{a} \quad , \tag{2-10}$$

we see that

$$\underline{e}_\xi = \frac{1}{d_1}(\underline{a} - \underline{s}) = \frac{1}{d_1}\left[(a_x - s_x)\,\underline{e}_x + (a_y - s_y)\,\underline{e}_y + a_z\,\underline{e}_z\right] , \tag{2-11}$$

so

$$\underline{e}_\xi = \frac{1}{d_1}\left[(\cos\phi_A \cos\lambda_A - s\cos\lambda_s)\,\underline{e}_x + (\cos\phi_A \sin\lambda_A - s\sin\lambda_s)\,\underline{e}_y + (\sin\phi_A)\,\underline{e}_z\right] . \tag{2-12}$$

If A' is the projection of A onto the (x,y)-plane, and d_2 is the distance from S to A', then

$$d_1 = (d_2^2 + \sin^2\phi_A)^{1/2} \quad , \tag{2-13}$$

by applying the cosine law to the triangle A'OS, we obtain

$$d_2 = \left[s^2 + \cos^2\phi_A - 2s\cos\lambda_A\cos(\lambda_A - \lambda_s)\right]^{1/2} \tag{2-14}$$

so

$$d_1 = \left[s^2 + 1 - 2s\cos\phi_A\cos(\lambda_A - \lambda_s)\right]^{1/2} \tag{2-15}$$

Next consider $\underline{e}_\eta$, which, because it lies in a plane that is normal to the equator and contains the ξ-axis, may be expressed as a linear combination of $\underline{e}_\xi$ and $\underline{e}_z$. The relevant geometry is shown in Figure 2-3, and we see that

$$\underline{e}_\eta = -(\tan\gamma)\,\underline{e}_\xi + (\sec\gamma)\,\underline{e}_z = -\left(\frac{\sin\phi_A}{d_2}\right)\underline{e}_\xi + \left(\frac{d_1}{d_2}\right)\underline{e}_z \quad , \tag{2-16}$$

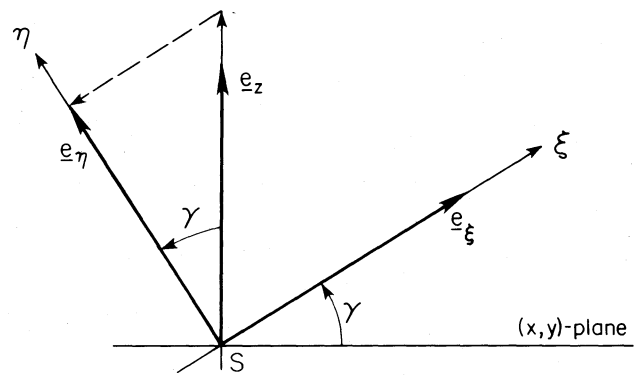

Figure 2-3. Relation between the unit vectors $\underline{e}_\xi$, $\underline{e}_z$, and $\underline{e}_\eta$.

where (from Fig. 2-1) γ is the angle between $\underline{e}_\xi$ and the (x,y)-plane. If we replace $\underline{e}_\xi$ in (2-16) by its representation in (2-12), we obtain

$$\underline{e}_\eta = \frac{1}{d_1 d_2} \Big[(-\sin\phi_A)(\cos\phi_A \cos\lambda_A - s\cos\lambda_s)\,\underline{e}_x - (\sin\phi_A)(\cos\phi_A \sin\lambda_A - s\sin\lambda_s)\,\underline{e}_y + d_2^2\,\underline{e}_z \Big] \quad . \tag{2-17}$$

Finally, $\underline{e}_\zeta$ can be obtained from the relation

$$\underline{e}_\zeta = \underline{e}_\xi \times \underline{e}_\eta \quad ; \tag{2-18}$$

when (2-16) is substituted into (2-18), we see that

$$\underline{e}_\zeta = \left(\frac{d_1}{d_2}\right)(\underline{e}_\xi \times \underline{e}_z) \quad , \tag{2-19}$$

which, on replacing $\underline{e}_\zeta$ by its representation (2-12), becomes

$$\underline{e}_\zeta = \frac{1}{d_2} \Big[(\cos\phi_A \sin\lambda_A - s\sin\lambda_s)\,\underline{e}_x - (\cos\phi_A \cos\lambda_A - s\cos\lambda_s)\,\underline{e}_y \Big] \quad . \tag{2-20}$$

Note that $\underline{e}_\zeta$ lies in the (x,y)-plane, as it should.

When (2-12), (2-17), and (2-20) are substituted into (2-8), and the result is equated to the right-side of (2-9), we obtain

$$\frac{t_x}{t} = \frac{1}{d_1 d_2} \left[(\cos \phi_A \cos \lambda_A - s \cos \lambda_s) (d_2 \cos \alpha - \sin \phi_A \sin \alpha \cos \omega) \right.$$

$$\left. + (\cos \phi_A \sin \lambda_A - s \sin \lambda_s) (d_1 \sin \alpha \sin \omega) \right] \quad , \tag{2-21a}$$

$$\frac{t_y}{t} = \frac{1}{d_1 d_2} \left[(\cos \phi_A \sin \lambda_A - s \sin \lambda_s) (d_2 \cos \alpha - \sin \phi_A \sin \alpha \cos \omega) \right.$$

$$\left. - (\cos \phi_A \cos \lambda_A - s \cos \lambda_s) (d_1 \sin \alpha \sin \omega) \right] \quad , \tag{2-21b}$$

and

$$\frac{t_z}{t} = \frac{1}{d_1} (\sin \phi_A \cos \alpha + d_2 \sin \alpha \cos \omega) \quad . \tag{2-21c}$$

To find the magnitude t of $\underline{t}$, we note that (since $\underline{f}$ is a unit vector)

$$\underline{f} \cdot \underline{f} = 1 = (\underline{s} + \underline{t}) \cdot (\underline{s} + \underline{t}) \tag{2-22}$$

which leads to the quadratic equation

$$t^2 + a_1 t + a_2 = 0 \quad , \tag{2-23}$$

where

$$a_1 = 2(\underline{s} \cdot \underline{t}) = 2\left(s_x \frac{t_x}{t} + s_y \frac{t_y}{t}\right) \tag{2-24a}$$

and

$$a_2 = s^2 - 1 \quad . \tag{2-24b}$$

When (2-2), (2-21a), and (2-21b) are substituted into (2-24a), we find that

$$a_1 = \frac{2s}{d_1 d_2} \left[(\cos \phi_A \cos(\lambda_A - \lambda_s) - s) (d_2 \cos \alpha - \sin \phi_A \sin \alpha \cos \omega) \right.$$

$$\left. + d_1 \cos \phi_A \sin(\lambda_A - \lambda_s) \sin \alpha \sin \omega \right] \quad . \tag{2-24c}$$

There is a rather obvious connection between the discriminant $a_1^2 - 4a_2$ of the quadratic equation (2-23) and the satellite-line-earth configuration. First, if $a_1^2 - 4a_2 < 0$, then (2-23) has no real root, and the specified line from the satellite does not intersect the earth at all. When $a_1^2 - 4a_2 > 0$, (2-23) has two real roots given by

$$t_1 = \frac{1}{2}\left[-a_1 - (a_1^2 - 4a_2)^{1/2}\right] \text{ and } t_2 = \frac{1}{2}\left[-a_1 + (a_1^2 - 4a_2)^{1/2}\right] \quad , \tag{2-25}$$

corresponding to the distances from S to the two points at which the line (characterized by the angles α, ω) intersects the spherical earth. Since t denotes the <u>magnitude</u> of a vector, we would expect that $t_1 > 0$ and $t_2 > 0$. If we note that

$$a_1 = 2(\underline{s} \cdot \underline{t})/t = 2s \cos(\pi - \psi) = -2s \cos \psi \quad , \tag{2-26}$$

where $\pi - \psi$ is the angle between $\underline{s}$ and $\underline{t}$, and ψ is the angle OSF in Figure 2-2, then for <u>any</u> point F on the earth (and any $s > 1$), we have $0 \leq \psi < \pi/2$, so $\cos \psi > 0$ and $a_1 < 0$. It then follows (since $|a_1| > (a_1^2 - 4a_2)^{1/2}$ when $a_1^2 - 4a_2 > 0$) that $t_1 > 0$ and $t_2 > 0$, as expected. We are, of course, interested only in the intersection point <u>nearer</u> S; i.e., the one illuminated by the satellite antenna, so we take the length of $\underline{t}$ to be the <u>smaller</u> of the two solutions t_1 and t_2, thus obtaining

$$t = \frac{1}{2}\left[-a_1 - (a_1^2 - 4a_2)^{1/2}\right] \quad . \tag{2-27}$$

We can now write the latitude ϕ_F and longitude λ_F of F as

$$\phi_F = \mathrm{Tan}^{-1}\left[\frac{f_z}{(f_x^2 + f_y^2)^{1/2}}\right] \tag{2-28}$$

and

$$\lambda_F = \tan^{-1}(f_y/f_x) \quad , \tag{2-29}$$

where, from (2-7),

$$f_x = s_x + (t_x/t)\, t \quad , \tag{2-30a}$$

$$f_y = s_y + (t_y/t)\, t \quad , \tag{2-30b}$$

and

$$f_z = (t_z/t)\, t \quad , \tag{2-30c}$$

with s_x and s_y being given by (2-2), t by (2-27), and t_x/t, t_y/t, and t_z/t by (2-21a), (2-21b), and (2-21c), respectively. The proper choice of inverse tangent in (2-29) is that which makes

$$\lambda_F = \text{Phase}(f_x + if_y) \quad , \tag{2-31}$$

where $-\pi < \lambda_F \leq \pi$. In FORTRAN computer programs, λ_F may be evaluated simply by calling the subroutine ATAN2 with arguments f_y and f_x (in that order).

2.4 Limb Line Calculations

There remains the case where $a_1^2 - 4a_2 = 0$ and the quadratic equation (2-23) has one (double) real root $t = -a_1/2$, corresponding to the situation in which the line from the satellite is tangent to the earth. In this event, $a_1 = -2a_2^{1/2}$, so the distance t from the satellite S to the point F of tangency is just

$$t = (s^2 - 1)^{1/2} \quad . \tag{2-32}$$

The locus of all such tangent points, i.e., those points on earth where the satellite is on the (idealized) observer horizon, is called the limb line, and may also be of interest.

One could, for an arbitrary given ω in the interval $(0, 2\pi)$, use (2-24c) to find the value of α for which $a_1^2 - 4(s^2 - 1) = 0$, then (setting $t = (s^2-1)^{1/2}$) compute the latitude and longitude of the corresponding limb line point using (2-28) and (2-29). However, this is the hard way, for α then depends on ω and one must solve (2-24c) for α for each point. It is much easier to note that the limb line is a (small) circle where the spherical earth is tangent to a right circular cone whose vertex is at S and whose axis lies along the line OS. All points on the limb line are, as we have see, a distance $(s^2 - 1)^{1/2}$ from S; furthermore, the location of the limb line is a function only of the satellite position S, being independent of the aim point A. For convenience, we thus let the aim point coincide with the sub-satellite point S'; i.e., we take $\phi_A = 0$ and $\lambda_A = \lambda_s$. Under these conditions, it follows from (2-14) and (2-15) that

$$d_1 = d_2 = s - 1 \quad , \tag{2-33}$$

as they should. Limb line points then correspond to a <u>single</u> value $\alpha = \alpha_L$ for <u>all</u> values of ω; from Figure 2-4, we see that

$$\sin \alpha_L = 1/s \quad \text{and} \quad \cos \alpha_L = (s^2 - 1)^{1/2}/s \quad . \tag{2-34}$$

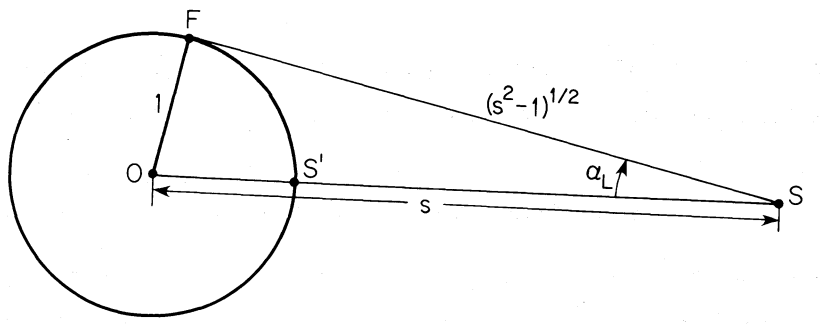

Figure 2-4. Geometry for limb line calculations.

For any prescribed ω in the interval $(0, 2\pi)$, the latitude ϕ_F and longitude λ_F of the corresponding limb line point F are given (as before) by (2-28) and (2-29), but now, on using (2-2), (2-32), (2-33), and (2-34), the expressions for f_x, f_y, and f_z become (after some simplification)

$$f_x = \frac{1}{s} \cos \lambda_s - \frac{(s^2 - 1)^{1/2}}{s} \sin \lambda_s \sin \omega \quad , \tag{2-35a}$$

$$f_y = \frac{1}{s} \sin \lambda_s + \frac{(s^2 - 1)^{1/2}}{s} \cos \lambda_s \sin \omega \quad , \tag{2-35b}$$

$$f_z = t_z = \frac{(s^2 - 1)^{1/2}}{s} \cos \omega \quad . \tag{2-35c}$$

Finally, we derive a simple criterion for deciding whether or not a given point A, whose latitude ϕ_A and longitude λ_A are prescribed, is illuminated by an antenna located on a specified geostationary satellite S. To do this, we regard the given point A as the aim point, then consider the special case where $\alpha = 0$; i.e., where F coincides with A. From (2-24c), it follows that

$$a_1 = - \frac{2s}{d_1} \left[s - \cos \phi_A \cos(\lambda_A - \lambda_s) \right] \quad , \tag{2-36}$$

which, after some algebra, leads to

$$a_1^2 - 4a_2 = \frac{4}{d_1^2} \left[s \cos \phi_A \cos(\lambda_A - \lambda_s) - 1 \right]^2 \quad . \tag{2-37}$$

When (2-37) vanishes, the point A is located on the limb line, this condition being equivalent to

$$\cos \phi_A \cos(\lambda_A - \lambda_s) = 1/s \quad . \tag{2-38}$$

From Figure 2-1, one can deduce that

$$\cos \phi_A \cos(\lambda_A - \lambda_s) = \cos \tau \quad , \tag{2-39}$$

where τ is the angle AOS; it then follows that the condition for A to be illuminated by the antenna at S is that $\tau \leq \tau_L$, τ_L being the value of τ when A is on the limb line. From Figure 2-4, we note that $\tau_L = \pi/2 - \alpha_L$ and $\cos \tau_L = \sin \alpha_L = 1/s$. Since $0 \leq \tau \leq \tau_L < \pi/2$ for illuminated points, our condition that A be illuminated is equivalent to

$$\cos \phi_A \cos(\lambda_A - \lambda_s) \geq 1/s \quad . \tag{2-40}$$

The negation of the relation (2-40) implies, of course, that the point A is not visible from the satellite.

As a check on our calculations, note that when $\alpha = 0$, it follows from (2-37) and (2-40) that for any illuminated aim point A,

$$(a_1^2 - 4a_2)^{1/2} = \frac{2}{d_1}\left[s \cos \phi_A \cos(\lambda_A - \lambda_s) - 1\right] \quad ; \tag{2-41}$$

on substituting (2-36) and (2-41) in (2-37), we find (as we should) that

$$t = \frac{1}{d_1}\left[s^2 + 1 - 2s \cos \phi_A \cos(\lambda_A - \lambda_s)\right] = d_1 \quad . \tag{2-42}$$

2.5 Footprint Calculations

The usual end result in a footprint generation procedure for a particular antenna is a map on which are portrayed the footprints corresponding to selected constant values of power density. In rather broad terms, one obtains this footprint map by (1) calculating, for each footprint, the locations (i.e., the geographical latitudes and longitudes) of a finite number of representative contour points, then (2) projecting these points onto the desired map, and (3) representing the footprints by a curve drawn through the projected contour points. In subsequent sections of this report, step (1) above will be considered in some detail for each of the idealized antenna models. Here, our discussion of the subject will concern certain features applicable to geostationary satellite antennas in general.

Within the geometric framework that we have established for describing earth/satellite/antenna configurations, let $\hat{P}(\alpha,\omega)$ denote the far-field power density pattern (normalized to a maximum of unity) of a given antenna located at S and having its main-beam axis directed toward a specific aim point A. The footprint corresponding to a constant power density $\hat{P}_o$ is then the intersection of the earth with a cone consisting of all straight lines from S whose directions are characterized by the angles (α,ω) satisfying the relation

$$\hat{P}(\alpha,\omega) = \hat{P}_o \quad . \tag{2-43}$$

Thus, when generating footprints for a specific antenna, one first determines (α,ω)-values for each of a finite number of representative cone elements corresponding to a prescribed $\hat{P}_o$; that is, one finds a suitable set of angle pairs (α_1,ω_1), ..., (α_N,ω_N) satisfying (2-43). In the usual approach to obtaining these angle pairs, one first specifies a suitable sequence ω_1, ..., ω_N of ω-values, then for each ω_j in the sequence, finds by some appropriate means the corresponding α_j that satisfies (2-43). One next applies (2-28), (2-29), and related formulas to calculate the geographic coordinates of the earth's intersection with each representative cone element.

The choice of ω-values in any particular situation depends on a variety of factors, in particular the character of the footprint itself. Suppose, as a first example, that the footprint consists of a simple closed curve about the main-lobe axis such that, as a point traverses the curve in one direction, the associated ω-values vary in a monotone fashion. This is equivalent to asserting, for the set of (α,ω) pairs satisfying (2-43), that α is a single-valued function of ω. Of course, α is also a periodic function of ω, the period being 2π radians; on physical grounds, one further argues that this function is continuous. Such footprints ordinarily occur, for instance, when the prescribed $\hat{P}_o$ is sufficiently large that the resulting contour reflects the simple structure of the well-defined main lobe of a typical satellite antenna. Suppose now in addition that the footprint is roughly circular in outline with the aim point near the center; then, as indicated in Figure 2-5(a), it is both convenient and optimum to choose a sequence of equi-spaced ω-values spanning an interval of 2π radians. If, on the other hand, the footprint is highly elongated in some direction, then as illustrated by Figure 2-5(b), such a choice of ω-values is not optimum, for it tends to under-determine the sharply curved "ends" of the footprint and/or over-determine (from the standpoint of computing

economy) the relatively flat "sides." Especially when computing or plotting economy is an important consideration, a better choice of ω-values in such a case would be one in which the representative points are more closely spaced where the footprint curves more rapidly. This is indicated in Figure 2-5(c), which shows the same footprint and the same <u>number</u> of representative points as in (b); that the modified arrangement of points results in an improved representation is apparent.

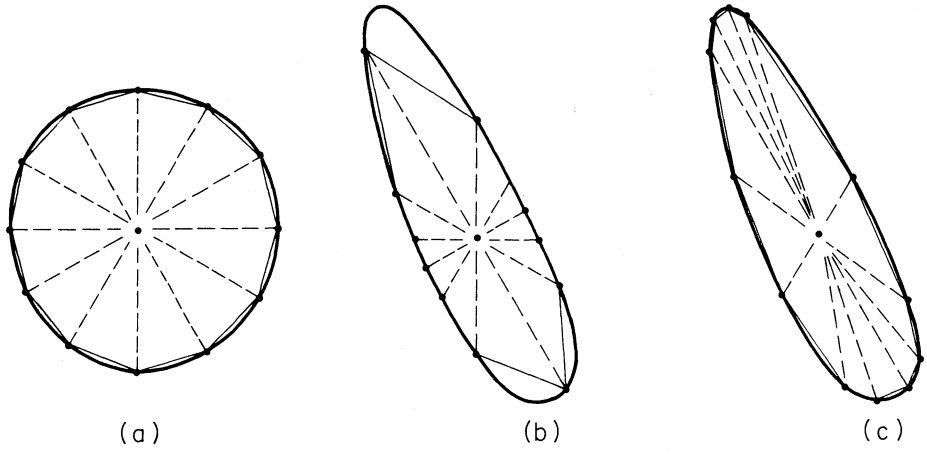

Figure 2-5. Footprints illustrating relation between contour shape and optimum arrangement of representative points.

As a more extreme example, suppose the prescribed $\hat{P}_o$ is sufficiently small that the resulting footprint reflects rather complex side-lobe structure of an antenna pattern. The footprint shown in Figure 2-6 is hypothetical, but illustrates the sort of features (such as fusing of somewhat irregular lobes) that one might in fact encounter, especially when dealing with the measured pattern of an actual antenna or the calculated pattern of a rather sophisticated model. As indicated in the figure, such footprints ordinarily consist of several simple closed curves, a particular one of which may or may not enclose the main-lobe axis. Note that in all cases where a particular curve does not enclose the main-lobe axis, and in some cases where it does, the variation of ω-values fails to be monotonic as a point traverses the curve. In other words, for the set of (α,ω) pairs corresponding to such a curve, α is not a single-valued function of ω. Then the choice of a monotone sequence of representative ω-values is obviously unsuitable; one must instead choose a sequence that is somehow "tailored" to the curve in question.

Choosing a distribution of representative contour points that is at least roughly optimum, while certainly desirable from economic considerations, is not

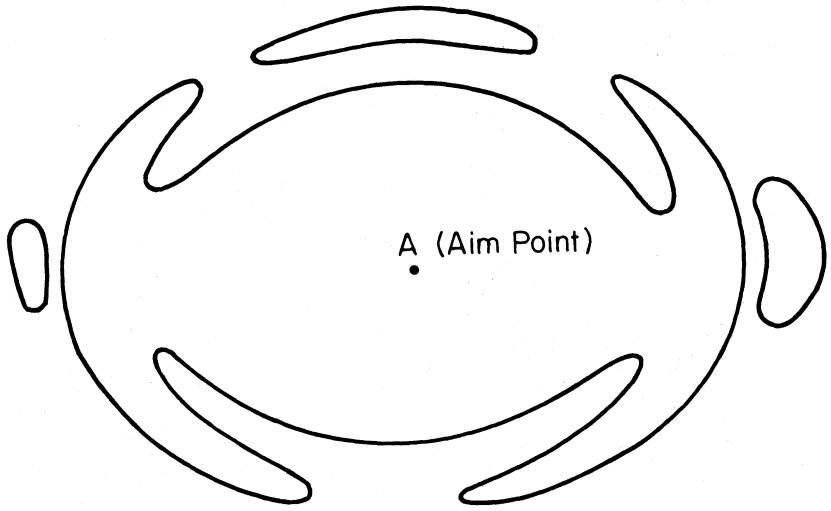

Figure 2-6. Hypothetical footprint reflecting complex side-lobe structure of antenna pattern.

always feasible. For example, the available data may severely limit the choice of ω-values for an actual antenna, or one may desire a single program to generate variously oriented footprints whose outlines can range from circular to highly elongated. The usual procedure in the latter case is to specify a sequence of ω-values that are equi-spaced and sufficiently close together to adequately represent the more sharply curving contour segments.

Besides the nature of the footprint itself, another important factor influencing the choice of representative contour points is the means by which the footprints are to be portrayed on maps. For instance, if footprints are to be drawn by hand, then each contour requires the locations of only relatively few representative points, typically ten to several tens, depending on contour complexity. Or, as a more likely example, suppose that one is producing footprint maps with a computer graphics system having one of a variety of point-plotting or vector-drawing devices. Then, if an accurate portrayal is desired, each contour requires the locations of a large number (usually several hundreds) of representative points. In this case, one should consider two alternative approaches. One is to generate

the entire plotter input by carrying out steps (1) and (2) as outlined in the first paragraph of this section. The other consists of calculating the locations of a much smaller number of contour points and then determining the required large number of intermediate points by some suitable interpolation procedure.

3. CIRCULAR APERTURE ANTENNAS

3.1 Introduction

For several varieties of practical transmitting antennas, the radiated fields may be regarded as issuing from a circular opening or aperture. Typical examples of such antennas include circular horns and lenses, and the widely used paraboloidal reflector or "parabolic dish." By an approximation which may range from good to rather crude, we simulate the main lobe of the far-field radiation pattern of such an antenna by that of a large, suitably illuminated curcular aperture in a conducting infinite plane.

As indicated in Figure 3-1, we consider a circular aperture of radius a lying in the (x,y)-plane and centered at the origin of a right-handed system of rectangular coordinates (x,y,z). Assume that $a \gg \lambda'$, where λ' is the free-space wavelength of the radiation illuminating the aperture; i.e., the aperture radius is several to many wavelengths. Assume also that the aperture field is linearly polarized, and has a uniform phase and circularly symmetric amplitude distribution $f(\rho)$, where ρ is the distance from the aperture center.

3.2 Radiation Patterns

If we take $f(\rho) = 0$ for $\rho > a$ (i.e., outside the aperture) and neglect edge effects, then under the above assumptions, the normalized far-field amplitude pattern may be approximated by

$$|\hat{F}(\Theta)| = |F(\Theta)/F(0)| \quad , \tag{3-1}$$

where $F(\Theta)$ is the surface integral (Silver, 1949, p. 173; Collin and Zucker, 1969)

$$F(\Theta) = \int_A f(\underline{\rho}) \exp(i\underline{k}\cdot\underline{\rho})\, dA \quad , \tag{3-2}$$

$\underline{k}$ is a vector of length $k = 2\pi/\lambda'$ in the direction of the observer, $\underline{\rho}$ is the position vector of a point (x,y) in the aperture, dA is an element of area containing (x,y), and the integration is extended over the surface A of the aperture. Note

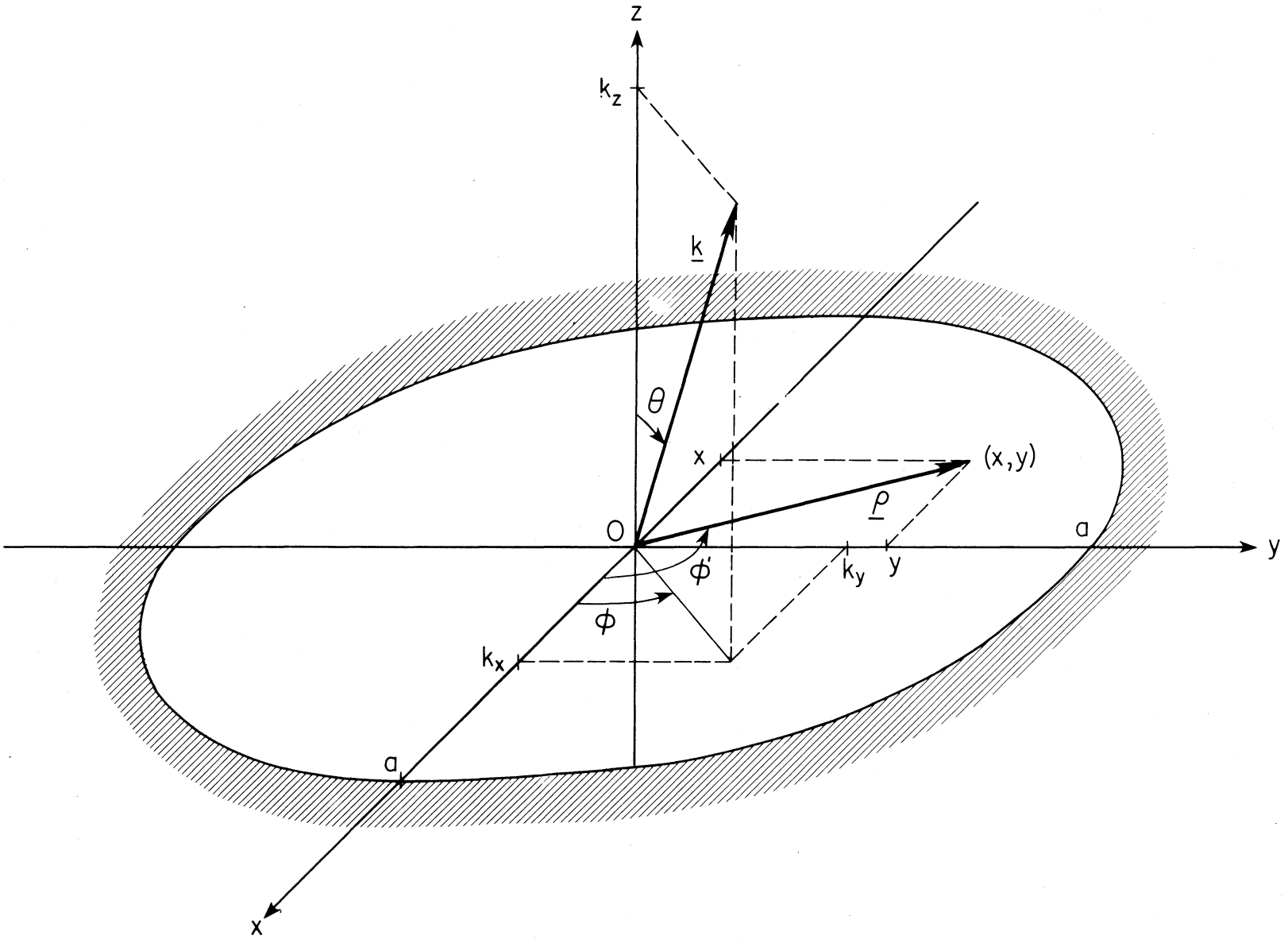

Figure 3-1. Geometry for the circular aperture antenna.

that, apart from a constant factor, $\hat{F}(\theta)$ is just the Fourier transform of the aperture field amplitude distribution $f(\rho)$. As we shall see, and as one would expect from the symmetry properties of the aperture illumination, it turns out that $\hat{F}(\theta)$ is independent of the azimuthal coordinate ϕ.

To facilitate the analysis, we also introduce plane polar coordinates (ρ,ϕ') which are related in the usual manner to x and y; i.e., by

$$x = \rho \cos \phi' \quad \text{and} \quad y = \rho \sin \phi' \quad .$$

Then, on noting that

$$\underline{k} = \underline{k}_{(x,y)} + \underline{k}_z \quad , \tag{3-3}$$

where $\underline{k}_{(x,y)}$ and $\underline{k}_z$ may be regarded as projections of $\underline{k}$ onto the (x,y)-plane and z-axis, respectively, we see that (since $\underline{\rho}$ in normal to $\underline{k}_z$

$$\underline{k} \cdot \underline{\rho} = \underline{k}_{(x,y)} \cdot \underline{\rho} = k\rho \sin \theta \cos(\phi - \phi') \quad , \tag{3-4}$$

so $F(\theta)$ may be written as the iterated integral

$$F(\theta) = \int_{\rho=0}^{a} f(\rho) \left\{ \int_{\phi'=0}^{2\pi} \exp\left[ik\rho \sin \theta \cos(\phi - \phi')\right] d\phi' \right\} \rho \, d\rho \quad . \tag{3-5}$$

To effect the integration on ϕ', one can start with the standard generating function expansion for Bessel functions of the first kind (e.g., Watson, 1944, p. 14-15), viz.

$$\exp\left[\frac{1}{2} u \left(t - \frac{1}{t}\right)\right] = \sum_{n=-\infty}^{\infty} J_n(u) \, t^n \quad . \tag{3-6}$$

Set

$$u = k\rho \sin \theta \text{ and } t = ie^{i(\phi-\phi')} \quad ;$$

then, after some algebra, one obtains

$$\exp\left[ik\rho \sin \theta \, \frac{e^{i(\phi-\phi')} + e^{-i(\phi-\phi')}}{2}\right] = J_o(k\rho \sin \theta) + 2 \sum_{n=1}^{\infty} i^n J_n(k\rho \sin \theta) \times \left(\frac{e^{in(\phi-\phi')} + e^{-in(\phi-\phi')}}{2}\right) \tag{3-7}$$

$$\exp\left[ik\rho \sin\theta \cos(\phi-\phi')\right] = J_o(k\rho \sin\theta) + 2 \sum_{n=1}^{\infty} i^n J_n(k\rho \sin\theta) \cos\left[n(\phi-\phi')\right] \quad . \tag{3-8}$$

Upon integrating both sides of (3-8) with respect to ϕ' over the interval $(0,2\pi)$, then interchanging the order of summation and integration on the right side (equivalent to term-by-term integration of the infinite series), and noting that

$$\int_o^{2\pi} \cos\left[n(\phi - \phi')\right] d\phi' = 0 \quad , \tag{3-9}$$

for $n = 1, 2, \ldots$, one finds that

$$\int_o^{2\pi} \exp\left[ik\rho \sin\theta \cos(\phi - \phi')\right] d\phi' = 2\pi J_o(k\rho \sin\theta) \quad . \tag{3-10}$$

When (3-10) is substituted into (3-5), we get the well-known result

$$F(\theta) = 2\pi \int_o^a f(\rho) J_o(k\rho \sin\theta) \rho \, d\rho \quad ; \tag{3-11}$$

since $J_o(0) = 1$, this leads to

$$\hat{F}(\theta) = \frac{\int_o^a f(\rho) J_o(k\rho \sin\theta) \rho \, d\rho}{\int_o^a f(\rho) \rho \, d\rho} \quad . \tag{3-12}$$

From the relations $0 \leq f(\rho) \leq 1$ and $\left|J_o(k\rho \sin\theta)\right| \leq 1$, it follows that

$$\left|F(\theta)\right| \leq 2\pi \int_o^a f(\rho) \left|J_o(k\rho \sin\theta)\right| \rho \, d\rho \leq 2\pi \int_o^a f(\rho) \rho \, d\rho \quad , \tag{3-13}$$

so $\left|F(\theta)\right| \leq \left|F(0)\right|$ and $\left|\hat{F}(\theta)\right| \leq 1$; further, because $\left|J_o(k\rho \sin\theta)\right| < 1$ when $0 < \rho \leq a$ and $0 < \theta \leq \pi/2$, we see that $\left|\hat{F}(\theta)\right| = 1$ only for $\theta = 0$. Thus, $\left|\hat{F}(\theta)\right|$ has a maximum (of unity) in a direction normal to the aperture plane, as it should for an aperture field with uniform phase (Silver, 1949, p. 176). Note also that $\hat{F}(\theta)$ in fact has the expected circular symmetry about the $\theta = 0$ axis.

Except for certain special forms of the aperture amplitude distribution $f(\rho)$, the pattern function $F(\theta)$ must be evaluated by some suitable means of numerical integration. The normalization factor $F(0)$ can be expressed in closed form for a much larger class of illumination functions $f(\rho)$, but in some cases, its calculation

also requires numerical integration. Observe that rather arbitrary aperture distributions can be used in (3-12), such as those designed to simulate aperture blocking, or ones that have been experimentally determined. Even though such functions may provide more realistic representations of actual aperture distributions, the model is still sufficiently idealized (e.g., the aperture field is assumed to be linearly polarized and to have uniform phase) that the resulting side lobes are unlikely to be an adequate approximation of real situation.

A "suitable means" of numerical integration depends to some extent on the nature of $f(\rho)$. It must, in any event, take into account the fact that the Bessel function $J_o(k\rho \sin\theta)$ may undergo several to many oscillations in the interval $(0,a)$. By way of example, the FOOTPRINTS program uses the aperture amplitude distribution

$$f(\rho) = \frac{1}{2}\left[1+T\right] + \frac{1}{2}\left[1-T\right] \cos\left(\frac{\pi\rho}{a}\right) \quad (0 \leq \rho \leq a) \quad , \qquad (3\text{-}14)$$

where the prescribed parameter T lies in the interval (0,1). A typical case of such a "raised cosine" distribution is sketched in Figure 3-2. Note that $f(\rho)$ has a maximum of unity at $\rho = 0$, so $T = f(a)$ is actually the ratio of the illumination amplitude at the edge of the aperture to that at the center. The aperture radius a and the illumination ratio T are specified by the program user; by setting $T = 1$, one obtains the case of uniform illumination.

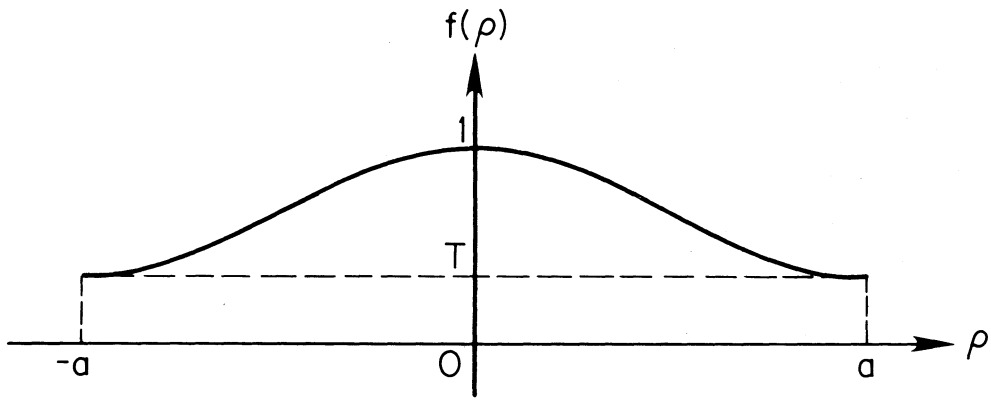

Figure 3-2. Typical aperture amplitude distribution used in FOOTPRINTS program for idealized circular aperture antenna.

The pattern normalization factor F(0) can be expressed in closed form, the integration being a straightforward exercise whose result is

$$F(0) = a^2\left[\frac{\pi}{2}(1+T) - \frac{2}{\pi}(1-T)\right] \quad . \tag{3-15}$$

The evaluation of $F(\theta)$ is effected by first dividing the interval (0,a) into a suitable number J of equal subintervals of length $\Delta\rho = a/J$, then writing

$$F(\theta) = 2\pi \sum_{j=1}^{J} \int_{(j-1)\Delta\rho}^{j\Delta\rho} f(\rho)\, J_o(k\rho \sin\theta)\rho\, d\rho \quad , \tag{3-16}$$

where $f(\rho)$ is given by (3-14). Each integral in the sum (3-16) is now approximated by the 8-point Gaussian quadrature formula

$$\int_{(j-1)\Delta\rho}^{j\Delta\rho} f(\rho)\, J_o(k\rho \sin\theta)\rho\, d\rho \approx \frac{1}{2}\Delta\rho \sum_{m=1}^{8} w_m\, f(\rho_{jm})\, J_o(k\rho_{jm} \sin\theta)\, \rho_{jm} \quad , \tag{3-17}$$

where

$$\rho_{jm} = \frac{1}{2}\Delta\rho(x_m + 2j - 1) \quad , \tag{3-18}$$

and x_m, w_m (m = 1, ..., 8) are Gaussian abscissas and weights, respectively. Using (3-14) - (3-18), the working formula for the normalized pattern function $\hat{F}(\theta)$ can be written as

$$\hat{F}(\theta) = \frac{\frac{\Delta\rho}{a^2}}{1 - \frac{4}{\pi^2}\frac{1-T}{1+T}} \sum_{j=1}^{J} \sum_{m=1}^{8} w_m\left[1 + \frac{1-T}{1+T}\cos\left(\frac{\pi\rho_{jm}}{a}\right)\right] J_o(k\rho_{jm} \sin\theta)\, \rho_{jm} \quad , \tag{3-19}$$

where $\Delta\rho = a/J$ and ρ_{jm} is given by (3-18). The number J is the largest integer not exceeding $1 + (ka \sin a)/\pi$; then $k\,\Delta\rho \sin\theta < \pi$, so the Bessel function $J_o(k\rho \sin\theta)$ does not undergo more than one-half an oscillation per subinterval.

An example of a useful aperture amplitude distribution $f(\rho)$ that leads to a closed-form expression for $\hat{F}(\theta)$ is the function (Sciambi, 1965)

$$f(\rho) = T + (1 - T)\left(1 - \frac{\rho^2}{a^2}\right)^{\nu} (0 \le \rho \le a) \quad , \tag{3-20}$$

where ν is an appropriate nonnegative constant and, as in the preceding example, T lies in the interval (0,1). Just as for the raised cosine distribution (3-14), the function in (3-20) has a maximum of unity at $\rho = 0$, so $T = f(a)$ is again the ratio of the illumination amplitude at the edge of the aperture to that at the center. When $\nu > 1$, the graph of (3-20) appears much like that of (3-14) for like values of a and T.

When (3-20) is substituted into (3-11) and the integration variable is transformed by the relation $\rho = a \sin t$, one obtains

$$F(\theta) = 2\pi a^2 T \int_0^{\pi/2} J_0(ka \sin\theta \sin t) \sin t \cos t \, dt + 2\pi a^2 (1-T) \int_0^{\pi/2} J_0(ka \sin\theta \sin t) \sin t \cos^{2\nu+1} t \, dt \quad . \tag{3-21}$$

Both of these integrals are special cases of what Watson (1944, p. 373) refers to as Sonine's first finite integral; the general formula also is given, for example by Abramowitz and Stegun (1964; 11.4.10, p. 485) and by Wheelon (1968; 1.364, p. 79). Its application leads to

$$F(\theta) = 2\pi a^2 \left[T \frac{J_1(ka \sin\theta)}{ka \sin\theta} + (1-T)\, 2^{\nu} \Gamma(\nu+1) \frac{J_{\nu+1}(ka \sin\theta)}{(ka \sin\theta)^{\nu+1}} \right] \quad , \tag{3-22}$$

where $\Gamma(\nu + 1)$ denotes the standard gamma function of argument $\nu + 1$. Noting that (Abramowitz and Stegun, 1964; 9.1.7, p. 360)

$$\lim_{\theta \to 0} \left(\frac{J_{\nu+1}(ka \sin\theta)}{(ka \sin\theta)^{\nu+1}} \right) = \frac{1}{2^{\nu+1}\, \Gamma(\nu+2)} \quad , \tag{3-23}$$

we find, after some algebra, that the pattern normalization factor is

$$F(0) = \pi a^2 \left(T + \frac{1-T}{\nu+1} \right) \quad ; \tag{3-24}$$

therefore,

$$\hat{F}(\theta) = \frac{2}{T + \frac{1-T}{\nu+1}} \left[T \frac{J_1(ka \sin\theta)}{ka \sin\theta} + (1-T)\, 2^{\nu} \Gamma(\nu+1) \frac{J_{\nu+1}(ka \sin\theta)}{(ka \sin\theta)^{\nu+1}} \right] \tag{3-25}$$

is the normalized pattern function. The paper by Sciambi (1965) includes a discussion of the relation between various antenna characteristics and the parameters ν, T.

3.3 Footprint Calculations for Circular Aperture Antennas

We consider now the problem of calculating, for an idealized circular aperture antenna on a geostationary satellite, the main-lobe footprint corresponding to a prescribed constant value $\hat{P}_s$ of normalized power density. We assume, of course, that the satellite longitude λ_s and aim point coordinates (ϕ_A, λ_A) are specified, as are the wavelength λ, the aperture radius a, and the circularly symmetric aperture amplitude distribution $f(\rho)$.

The geometry used to describe circular aperture antenna patterns is fitted into that used in section 2 to describe the antenna/satellite/earth configuration by identifying the positive z-axis of Figure 3-1 with the positive ξ-axis of Figure 2-1. The antenna's main-beam axis is then directed toward the aim point A, and the angle θ in Figure 3-1 is identified with the angle α in section 2. Because the far-field pattern of our idealized circular aperture antenna has circular symmetry about the main-beam axis, the relation of the x and y axes in Figure 3-1 to the η and ζ axes in Figure 2-1 is immaterial.

This circular symmetry also greatly simplifies the task of calculating the locations of representative contour points. Note that the "main lobe" portion of the cone corresponding to a constant power density $\hat{P}_s$ is a right circular cone whose apex angle (i.e., the angle from the cone (antenna beam axis to any element or generator) is the "main-lobe" root α_s of

$$\hat{P}(\alpha) = \hat{P}_s \quad . \tag{3-26}$$

For any suitable sequence $\omega_1, \omega_2, \ldots, \omega_N$ of ω-values, representative cone elements are thus characterized by the angle pairs $(\omega_1, \alpha_s), (\omega_2, \alpha_s), \ldots, (\omega_N, \alpha_s)$. One then proceeds in the standard way to calculate the geographical coordinates of the resulting contour points by applying (2-28), (2-29), and related formulas. Observe that the footprint outlines may range from circular (when the aim point coincides with the sub-satellite point) to highly elongated (when the antenna beamwidth is narrow and the aim point is near the limb line). In view of the relative simplicity of the calculations once the necessary α_s has been evaluated, one usually can ignore the optimization of representative contour points, and simply choose a monotone sequence of equi-spaced ω-values that span the internal $(0, 2\pi)$ and are sufficiently numerous to adequately define the footprint.

It is not ordinarily possible to write down a formula for solutions of (3-26), as is illustrated by the particularly simple instance of uniform aperture illumination, which leads to the equation

$$\left[\frac{J_1(ka \sin \alpha)}{1/2\ ka \sin \alpha}\right]^2 = \hat{P}_s \tag{3-27}$$

Hence, obtaining a numerical approximation to the value of α_s, corresponding to a specified power density $\hat{P}_s$, generally requires some sort of iterative root-finding procedure.

A typical graph of $\hat{P}(\alpha)$ vs. α is shown in Figure 3-3 for an idealized circular aperture antenna. Note that the lobes of the pattern are well-defined; i.e., all inter-lobe nulls are actually zero. When $\hat{P}_s$ exceeds the greatest side-lobe maximum (of which we usually have, however, no a priori knowledge), then α_s is the <u>only</u> positive root of (3-26), and its numerical approximation is quite straightforward by any of several standard procedures. In the contrary case, however, we see that (3-26) has additional (positive) solutions that correspond to side lobes; for example, if the specified power density is $\hat{P}'_s$ in Figure 3-3, then besides the "main-lobe" root α'_s, (3-26) has the roots α'_{sA} and α'_{sB}. In such cases, there exists the problem of devising a computer routine which will reliably converge to the desired main lobe root α_s, rather than to one of the (larger) side-lobe roots.

This difficulty often can be mitigated, but not eliminated, by solving instead the equivalent equation

$$\hat{F}(\alpha) = \hat{P}_s^{1/2} \quad . \tag{3-28}$$

As indicated in Figure 3-4, this equation has no solutions corresponding to the first, third, etc. side lobes, leaving one to contend with unwanted roots only for even-order side lobes.

Our approach to approximating the value of the "main-lobe" root α_S of (3-28) consists of two parts. The first is isolating α_S in an interval (α_L, α_R); i.e., finding an interval (α_L, α_R) that contains α_S, but no other ("side-lobe") root of (3-28). The second part is successively applying either the standard bisection method or the modified false position method to compute approximations α_{Sj} $(j = 1,2, \ldots, J)$ to α_S until $|\hat{F}(\alpha_{SJ}) - \hat{P}_S^{1/2}|$ is less than some specified small number $\delta\hat{F}$.

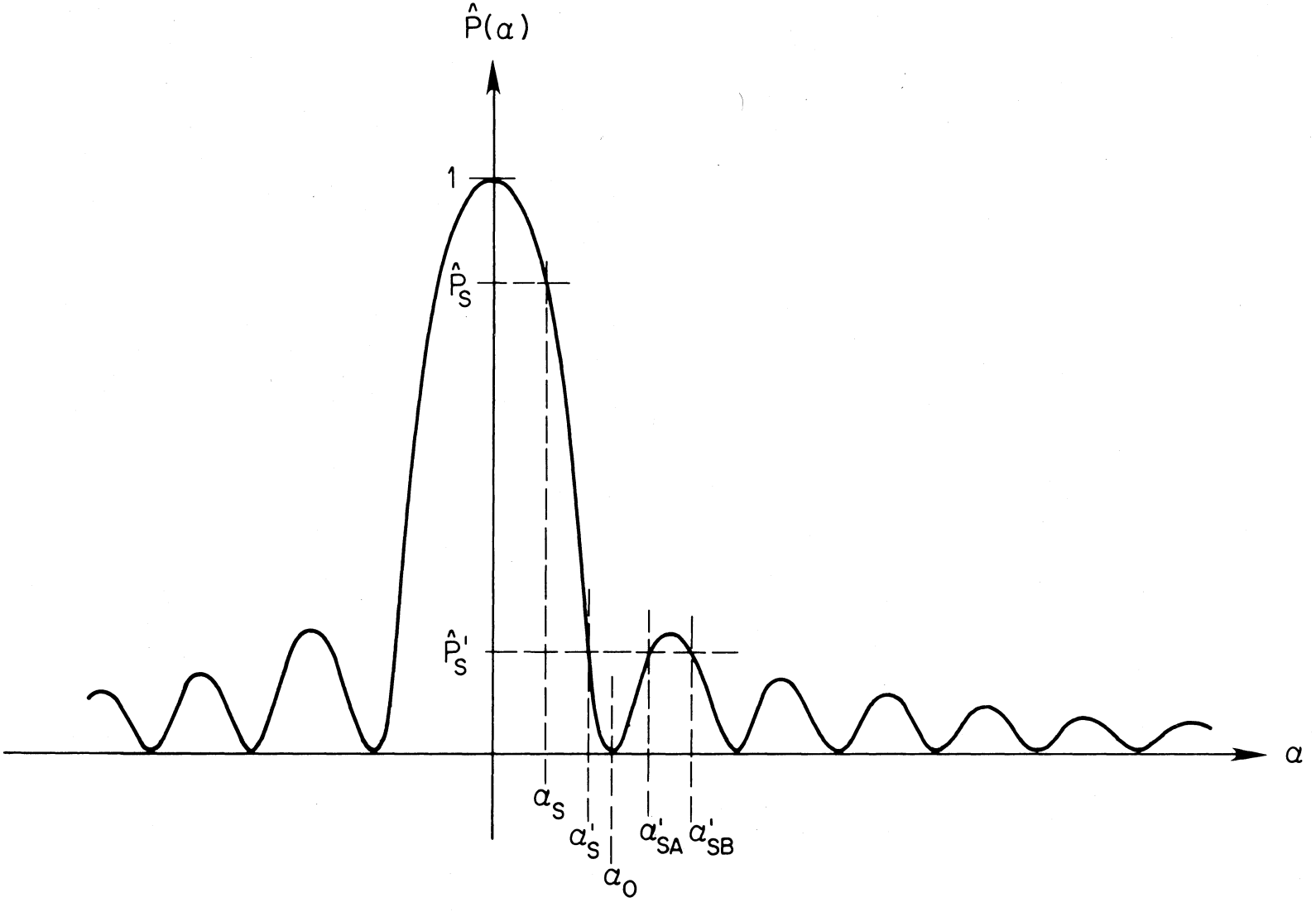

Figure 3-3. Typcial plot of normalized far-field power density $\hat{P}(\alpha)$ vs. off-axis angle α for an idealized circular aperture antenna.

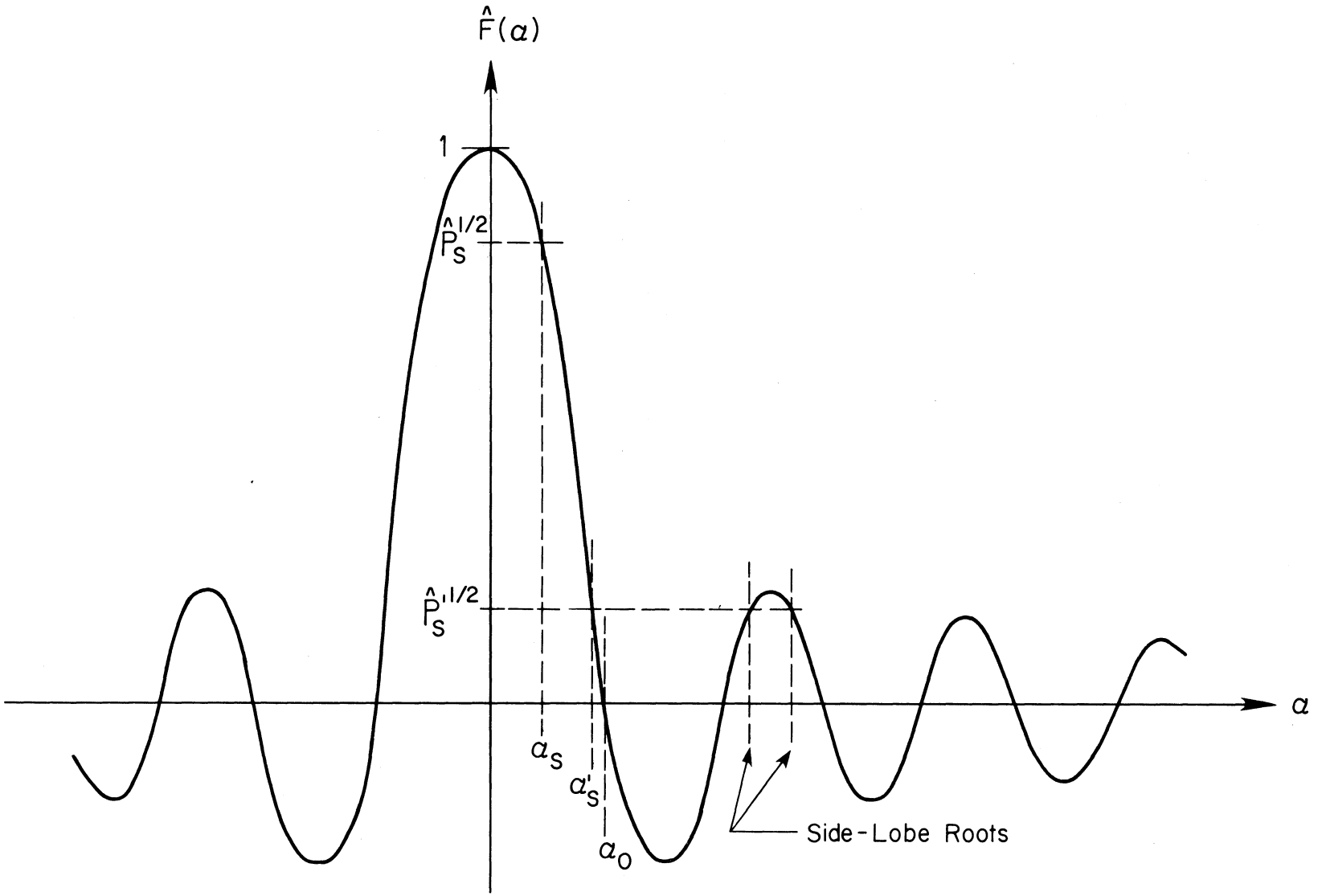

Figure 3-4. Typical plot of normalized far-field amplitude function $\hat{F}(\alpha)$ vs. off-axis angle α for an idealized circular aperture antenna.

In certain circumstances, one may be able to determine an interval (α_L, α_R) at the outset. For example, in the case of uniform aperture illumination, where we seek α_S satisfying

$$\frac{J_1(ka \sin \alpha)}{1/2\ ka \sin \alpha} = \hat{P}_S^{1/2} \quad , \tag{3-29}$$

we know that (for $0 < \hat{P}_S < 1$) $0 < \alpha_S < \alpha_0$, where α_0 is the angular position of the pattern's first null. Thus,

$$ka \sin \alpha_0 = j_{1,1} \quad , \tag{3-30}$$

where $j_{1,1} \approx 3.83171$ is the smallest positive zero of the Bessel function J_1; hence,

$$\alpha_0 = \sin^{-1}\left(\frac{j_{1,1}}{ka}\right) \quad . \tag{3-31}$$

In the more usual case, where α_0 cannot be easily obtained, we employ a systematic search to find an interval (α_L, α_R) that isolates α_S. Note that if $0 \leq \hat{P}_S < 1$, then $\hat{F}(\alpha) > \hat{P}_S^{1/2}$ for <u>all</u> α such that $0 \leq \alpha < \alpha_S$; furthermore, $\hat{F}(\alpha) < \hat{P}_S^{1/2}$ for all $\alpha > \alpha_S$ in <u>some</u> neighborhood of α_S. So, for some well-chosen step size $\Delta\alpha$, we simply compute in succession the function values $\hat{F}(m\Delta\alpha)$ for $m=1, 2, \ldots, M$, comparing each with $\hat{P}_S^{1/2}$ and stopping the computations at the smallest (positive) integer M such that $\hat{F}(M\Delta\alpha) \leq \hat{P}_S^{1/2}$. In the (unlikely) event that $\hat{F}(M\Delta\alpha) = \hat{P}_S^{1/2}$, then $\alpha_S = M\Delta\alpha$ and our root-finding is done; otherwise, set $\alpha_L = (M-1)\Delta\alpha$ and $\alpha_R = M\Delta\alpha$.

If the specified power $\hat{P}_S$ exceeds the greatest side-lobe maximum, then the foregoing procedure works well for a rather wide range of $\Delta\alpha$-values. In the contrary case, however, where "side-lobe" roots exist, there is a fairly obvious pitfall. Although the interval (α_L, α_R) certainly contains a root of (3-29), it does not necessarily contain α_S; and even if it <u>does</u> contain α_S, there is no guarantee that it does not also contain side-lobe roots. If the step-size $\Delta\alpha$ is less than the angular width of the first side lobe, then α_S is indeed isolated as desired in (α_L, α_R). (Ideally, for the sake of computing economy, $\Delta\alpha$ should be only slightly smaller than the first side-lobe width.) Unfortunately, however, one generally has no a priori knowledge of the angular width of any lobe, so the choice of $\Delta\alpha$ becomes a matter of judgement, more or less informed by experience. Evaluating the wrong root of (3-28) is apt to be a more serious fault than simply

failing to minimize computer time, so it is usually better to choose $\Delta\alpha$ unnecessarily small in order to increase the likelihood of isolating α_S. One might, for example, take $\Delta\alpha$ to be $\alpha_0/10$, where α_0 is given by (3-31). In situations where one suspects a problem, or where many footprints are to be generated for a particular antenna, it is wise to undertake a detailed calculation of the pattern structure in order to obtain an accurate estimate of α_0, rather than to rely on the step-wise search outlined above.

Generalized flowcharts for algorithms that implement the bisection and modified false position methods are shown in Figures 3-5 and 3-6, respectively. In the latter (Hamming, 1971; Conte and deBoor, 1965),

$$\alpha_C = \frac{\alpha_R H_L - \alpha_L H_R}{H_L - H_R} \quad , \tag{3-32}$$

$$H_L = H(\alpha_L), \quad H_C = H(\alpha_C), \quad H_R = H(\alpha_R) \quad , \tag{3-33}$$

where

$$H(\alpha) = \hat{F}(\alpha) - \hat{P}_S^{1/2} \quad . \tag{3-34}$$

The bisection method is particularly simple and effective, but tends to be somewhat slow; the modified false position method is generally faster, equally effective, and only slightly less simple.

In practice, specified power levels are often expressed in decibels relative to the main-beam maximum; that is, one is given

$$\hat{P}_{Sdb} = 10 \log_{10}(\hat{P}_S) \quad , \tag{3-35}$$

so that

$$\hat{P}_S^{1/2} = (10)^{\hat{P}_{Sdb}/20} = \exp\left[(\hat{P}_{Sdb}/20) \log_e 10\right] \quad . \tag{3-36}$$

4. ELLIPTICAL APERTURE ANTENNAS

4.1 Introduction

Through an approach analogous to that employed for circular aperture antennas, we simulate the main lobe of the far-field radiation pattern of certain antennas by that of a large, suitably illuminated elliptical aperture in a conducting in-

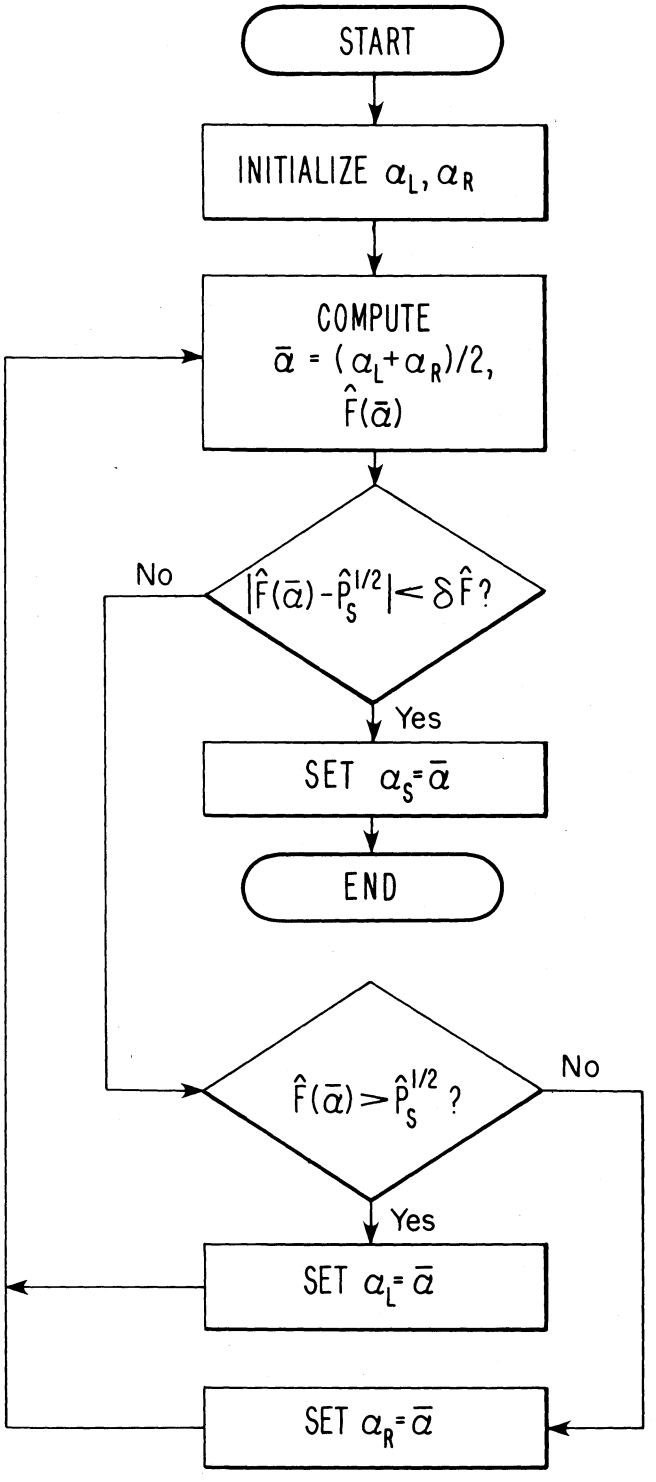

Figure 3-5. Generalized flowchart for an algorithm implementing bisection method of evaluating α_S.

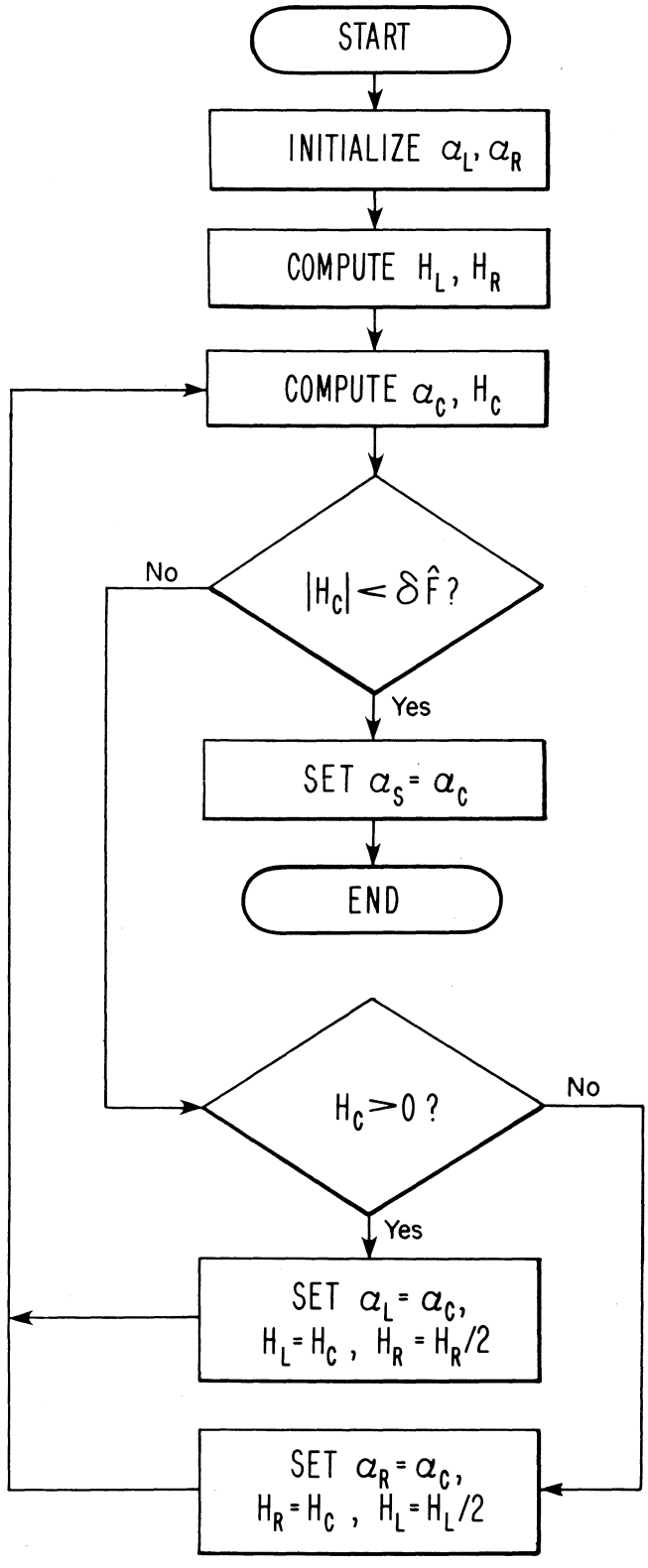

Figure 3-6. Generalized flowchart for an algorithm implementing modified false position method of evaluating α_S.

finite plane. As indicated in Figure 4-1, the aperture lies in the z=0 plane and is centered at the origin or a right-handed system of rectangular coordinates (x,y,z); the aperture boundary is the ellipse

$$\frac{x^2}{a^2} + \frac{y^2}{b^2} = 1 \quad . \tag{4-1}$$

For later convenience in specifying the antenna's orientation, we somewhat arbitrarily require that $a \geq b$, so the aperture's major axis lies along the x-axis of our coordinate system. Assume that $a \gg \lambda'$ and $b \gg \lambda'$, λ' being the free-space wavelength of the radiation illuminating the aperture; i.e., both axes of the aperture are several to many wavelengths long. Assume also that the aperture field is linearly polarized and has a uniform phase and a separable amplitude distribution f(x,y) of the form

$$f(x,y) = X(x)\ Y(y) \quad , \tag{4-2}$$

where X(x) is a function of x only and Y(y) is a function of y only (Silver, 1949, p. 182).

By taking a=b, one may be able to simulate main-lobe patterns of certain circular aperture antennas whose illumination distributions lack circular symmetry. By the same token, it is not generally possible to represent a circularly symmetric illumination distribution by a function of the form (4-2). Indeed, by noting that a circularly symmetric function f is characterized by the condition $\partial f/\partial\phi \equiv 0$ (where (r,ϕ) are the usual polar coordinates about the aperture center), it is a routine exercise to show, if the distribution f(x,y) in (4-2) has circular symmetry, that X(x) and Y(y) must be proportional to $e^{\alpha x^2}$ and $e^{\alpha y^2}$, respectively, where α is a constant. Observe that $\alpha = 0$ corresponds to a uniformly illuminated aperture.

4.2 Radiation Patterns

As before, we assume that the illumination distribution f(x,y) = 0 outside the aperture and neglect edge effects, so the normalized far-field amplitude pattern may be approximated by

$$|\hat{F}(\theta,\phi)| = |F(\theta,\phi)/F(0,\phi)| \quad , \tag{4-3}$$

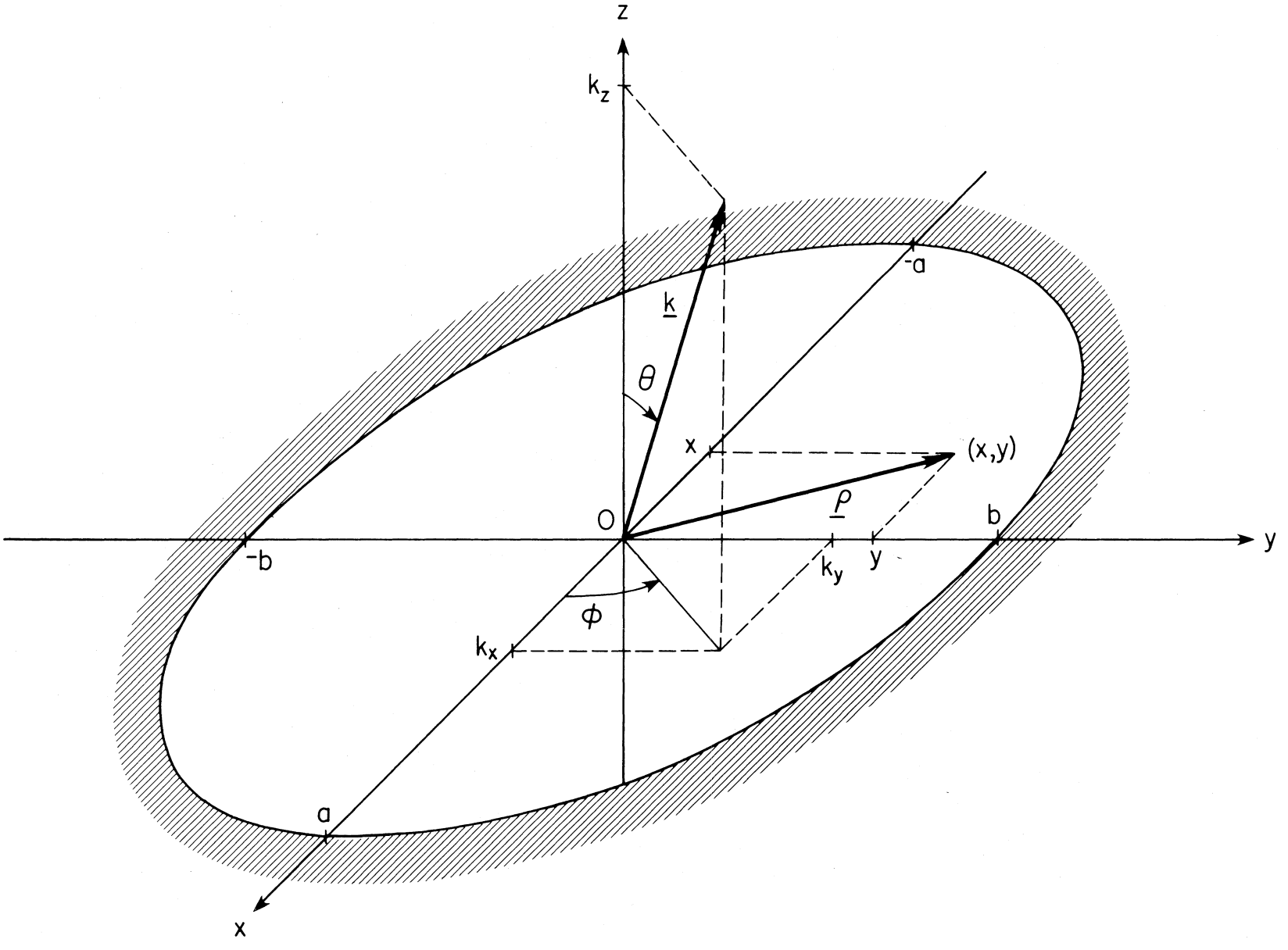

Figure 4-1. Geometry for the elliptical aperture antennas.

where $F(\theta,\phi)$ is the surface integral (Silver, 1949, p. 173; Collin, 1969)

$$F(\theta,\phi) = \int_A f(x,y) \exp(i\underline{k} \cdot \underline{\rho})\, dA \quad , \tag{4-4}$$

$\underline{k}$ is a vector of length $k = 2\pi/\lambda'$ in the direction of the observer, $\underline{\rho}$ is the position vector of a point (x,y) in the aperture, dA is an element of area containing (x,y), and the integration is extended over the surface A of the aperture. Of course, it is also the case here that, apart from a constant factor, $\hat{F}(\theta,\phi)$ is the Fourier transform of the aperture field amplitude distribution $f(x,y)$.

From Figure 4-1, note that

$$\underline{k} \cdot \underline{\rho} = k_x\, x + k_y\, y \quad , \tag{4-5}$$

where

$$k_x = k \sin\theta \cos\phi \tag{4-6a}$$

and

$$k_y = k \sin\theta \sin\phi \quad . \tag{4-6b}$$

Substituting (4-2) and (4-5) into (4-4) gives

$$F(\theta,\phi) = \int_A X(x)\, Y(y) \exp\left[i(k_x x + k_y y)\right] dA \quad , \tag{4-7}$$

which may also be written as the iterated integral

$$F(\theta,\phi) = \int_{x=-a}^{+a} X(x) \exp(ik_x x) \left\{ \int_{y=-b\,h(x)}^{+b\,h(x)} Y(y) \exp(ik_y y)\, dy \right\} dx \quad , \tag{4-8}$$

where

$$h(x) = \left(1 - \frac{x^2}{a^2}\right)^{1/2} \quad . \tag{4-9}$$

Except for certain special forms of the functions $X(x)$ and $Y(y)$, one must evaluate $F(\theta,\phi)$ (and $F(\theta,\phi)$) by means of numerical integration.

4.3 A Special Case

Useful examples of "certain special forms" of the functions $X(x)$ and $Y(y)$ are given by Adams and Kelleher (1950), who let

$$X(x) = \sum_{m=0}^{M} p_m \cos\left(\frac{m\pi x}{a}\right) \tag{4-10a}$$

and

$$Y(y) = \sum_{n=0}^{N} q_n \cos\left(\frac{n\pi y}{b}\right) \quad . \tag{4-10b}$$

By a proper choice of coefficients p_m and q_n, most practical illumination distributions can be adequately approximated by using only a few terms in (4-10a) and (4-10b). When $X(x)$ and $Y(y)$ are expressed in this way, $F(\theta,\phi)$ can be evaluated as a linear combination of Λ_1 functions, where in terms of the more familiar Bessel function J_1,

$$\Lambda_1(u) = (2/u)\ J_1(u) \quad . \tag{4-11}$$

The explicit form of $F(\theta,\phi)$, along with an outline of its derivation, will be given in this section, as neither were included in the brief paper by Adams and Kelleher (1950).

When (4-10a) and (4-10b) are substituted into (4-8), $F(\theta,\phi)$ may be written as a sum of iterated integrals

$$F(\theta,\phi) = \sum_{m=0}^{M} \sum_{n=0}^{N} p_m\, q_n\, S_{mn} \quad , \tag{4-12}$$

where

$$S_{mn} = \int_{x=-a}^{+a} \exp(ik_x x)\ \cos\left(\frac{m\pi x}{a}\right) \left\{ \int_{y=-bh(x)}^{+bh(x)} \exp(ik_y y)\ \cos\left(\frac{n\pi y}{b}\right) dy \right\} dx \quad , \tag{4-13}$$

and $h(x)$ is given by (4-9). On introducing a new integration variable t by means of the relation $x = a \cos t$, the expression for S_{mn} becomes

$$S_{mn} = a \int_{t=0}^{\pi} \exp(ik_x a \cos t)\ \cos(m\pi \cos t) \left\{ \int_{y=-b\sin t}^{+b\sin t} \exp(ik_y y) \cos\left(\frac{n\pi y}{b}\right) dy \right\} \sin t\ dt \quad . \tag{4-14}$$

The integration on y is a standard form that may be evaluated in any of several ways, the various results being equivalent to

$$\int_{-b\sin t}^{+b\sin t} \exp(ik_y y) \cos\left(\frac{n\pi y}{b}\right) dy = \frac{b}{k_y b + n\pi} \sin\left[(k_y b + n\pi) \sin t\right]$$

$$+ \frac{b}{k_y b - n\pi} \sin\left[(k_y b - n\pi) \sin t\right] . \qquad (4\text{-}15)$$

Substituting (4-15) into (4-14) leads to

$$S_{mn} = \frac{ab}{k_y b + n\pi} \int_0^\pi \exp(ik_x a \cos t) \cos(m\pi \cos t) \sin\left[(k_y b + n\pi) \sin t\right] \sin t \, dt$$

$$+ \frac{ab}{k_y b - n\pi} \int_0^\pi \exp(ik_x a \cos t) \cos(m\pi \cos t) \sin\left[(k_y b - n\pi) \sin t\right] \sin t \, dt , \qquad (4\text{-}16)$$

or, if one uses the complex exponential representation of $\cos(m\pi \cos t)$,

$$S_{mn} = \frac{ab/2}{k_y b + n\pi} \left\{ \int_0^\pi \exp\left[i(k_x a + m\pi) \cos t\right] \sin\left[(k_y b + n\pi) \sin t\right] \sin t \, dt \right.$$

$$\left. + \int_0^\pi \exp\left[i(k_x a - m\pi) \cos t\right] \sin\left[(k_y b + n\pi) \sin t\right] \sin t \, dt \right\}$$

$$+ \frac{ab/2}{k_y b - n\pi} \left\{ \int_0^\pi \exp\left[i(k_x a + m\pi) \cos t\right] \sin\left[(k_y b - n\pi) \sin t\right] \sin t \, dt \right.$$

$$\left. + \int_0^\pi \exp\left[i(k_x a - m\pi) \cos t\right] \sin\left[(k_y b - n\pi) \sin t\right] \sin t \, dt \right\} . \qquad (4\text{-}17)$$

Each of the integrals in (4-17) is of the form

$$S(u,v) = \int_0^\pi \exp(iu \cos t) \sin(v \sin t) \sin t \, dt \quad , \qquad (4\text{-}18)$$

which can be evaluated by differentiating the relation (Gray, et al., 1922)

$$\int_0^\pi \exp(iu \cos t) \cos(v \sin t) \, dt = \pi J_o\left(\left[u^2 + v^2\right]^{1/2}\right) \qquad (4\text{-}19)$$

with respect to v. The result is

$$S(u,v) = \int_0^\pi \exp(iu \cos t) \sin(v \sin t) \sin t \, dt = \pi v \frac{J_1\left(\left[u^2 + v^2\right]^{1/2}\right)}{\left[u^2 + v^2\right]^{1/2}} \qquad (4\text{-}20a)$$

or

$$S(u,v) = (\pi v/2)\ \Lambda_1([u^2 + v^2]^{1/2}) \quad . \tag{4-20b}$$

On using (4-20a), the expression for S_{mn} can be written as

$$S_{mn} = \frac{\pi ab}{4}\Big\{\Lambda_1([k_x a + m\pi)^2 + (k_y b + m\pi)^2]^{1/2}) + \Lambda_1([k_x a - m\pi)^2 + (k_y b + n\pi)^2]^{1/2})$$
$$+ \Lambda_1([k_x a + m\pi)^2 + (k_y b - n\pi)^2]^{1/2}) + \Lambda_1([(k_x a - m\pi)^2 + (k_y b - n\pi)^2]^{1/2})\Big\} \quad . \tag{4-21}$$

When the coefficients p_m and q_n are specified, (4-12) and (4-21), along with (4-6a) and ((4-6b), are the working formulas for evaluating $F(\theta,\phi)$. To calculate $F(0,\phi)$, note from (4-6a) and (4-6b) that $k_x = k_y = 0$ when $\theta = 0$; the formula for S_{mn} then reduces to

$$S_{mn}(0,\phi) = \pi ab\ \Lambda_1(\pi[m^2 + n^2]^{1/2}) \quad . \tag{4-22}$$

As a particular example, to simulate elliptical aperture antennas in program FOOTPRINTS, we choose

$$X(x) = \frac{1}{2}(1 + T_a) + \frac{1}{2}(1 - T_a)\cos\left(\frac{\pi x}{a}\right)(-a \le x \le a) \tag{4-23a}$$

and

$$Y(y) = \frac{1}{2}(1 + T_b) + \frac{1}{2}(1 - T_b)\cos\left(\frac{\pi y}{b}\right)(-b \le y \le b) \quad , \tag{4-23b}$$

where the prescribed parameters T_a, T_b both lie in the interval (0,1). This choice is equivalent, of course, to taking $M = 1$, $P_o = \frac{1}{2}(1 + T_a)$, $P_1 = \frac{1}{2}(1 - T_a)$ in (4-10a), and $N = 1$, $q_0 = \frac{1}{2}(1 + T_b)$, $q_1 = \frac{1}{2}(1 - T_b)$ in (4-10b). The physical significance of T_a, T_b is analogous to that of the parameter T for the idealized circular aperture antenna. That is, since $X(0) = Y(0) = f(0,0) = 1$ and $X(\pm a) = T_a$, $Y(\pm b) = T_b$, we see that T_a and T_b are the ratios of the illumination amplitude at the ends of the respective aperture axes to that at the center. Taking $T_a = T_b = 1$ corresponds to a uniformly illuminated elliptical aperture.

When (4-23a) and (4-23b) are used in (4-12), the resulting expression for the normalized far-field amplitude pattern $\hat{F}(\theta,\phi)$ can be written as

$$\hat{F}(\theta,\phi) = \Big\{ \Lambda_1\left(\left[(k_x a)^2 + (k_y b)^2\right]^{1/2}\right)$$

$$+ \frac{1}{2}\frac{1-T_b}{1+T_b}\left[\Lambda_1\left(\left[(k_x a)^2 + (k_y b+\pi)^2\right]^{1/2}\right) + \Lambda_1\left(\left[(k_x a)^2 + (k_y b-\pi)^2\right]^{1/2}\right)\right]$$

$$+ \frac{1}{2}\frac{1-T_a}{1+T_a}\left[\Lambda_1\left(\left[(k_x a+\pi)^2 + (k_y b)^2\right]^{1/2}\right) + \Lambda_1\left(\left[(k_x a-\pi)^2 + (k_y b)^2\right]^{1/2}\right)\right]$$

$$+ \frac{1}{4}\frac{1-T_a}{1+T_a}\,\frac{1-T_b}{1+T_b}\left[\Lambda_1\left(\left[(k_x a+\pi)^2 + (k_y b+\pi)^2\right]^{1/2}\right) + \Lambda_1\left(\left[(k_x a-\pi)^2+(k_y b+\pi)^2\right]^{1/2}\right)\right.$$

$$\left. + \Lambda_1\left(\left[(k_x a+\pi)^2 + (k_y b-\pi)^2\right]^{1/2}\right) + \Lambda_1\left(\left[(k_x a-\pi)^2+(k_y b-\pi)^2\right]^{1/2}\right)\right]\Big\}$$

$$\times \left\{1 + \left[\frac{1-T_a}{1+T_a} + \frac{1-T_b}{1+T_b}\right]\Lambda_1(\pi) + \frac{1-T_a}{1+T_a}\,\frac{1-T_b}{1+T_b}\,\Lambda_1(\pi\sqrt{2})\right\}^{-1} \qquad (4\text{-}24)$$

Note that for the uniformly illuminated aperture, we have $T_a = T_b = 1$,

$$\hat{F}(\theta,\phi) = \Lambda_1\left(\left[(k_x a)^2 + (k_y b)^2\right]^{1/2}\right) \quad . \qquad (4\text{-}25)$$

Further, when $a = b$, $(k_x a)^2 + (k_y b)^2 = a^2(k_x^2 + k_y^2) = (ka \sin\theta)^2$, and (4-25) becomes

$$\hat{F}(\theta,\phi) = \Lambda_1(ka \sin\theta) \quad ,$$

which is, as it should be, the result for a uniformly illuminated circular aperture.

4.4 Footprint Calculations for Elliptical Aperture Antennas

The geometry for describing elliptical aperture antenna patterns (Fig. 4-1) is related to that used to describe the antenna/satellite/earth configuration (Fig. 2-1) by first identifying the positive z-axis in Figure 4-1 with the positive ξ-axis in Figure 2-1. The antenna's main-beam axis is then directed toward the aim point A. The orientation of the elliptical aperture about the main-beam axis is defined, as illustrated in Figure 4-2, by specifying the angle β from the positive η-axis to the major axis of the aperture (i.e., the $\phi = 0$ or positive x-axis in Fig. 4-1). The angles α, ω in section 2 are then related to the angles θ, ϕ in Figure 4-1 by $\alpha = \theta$ and $\omega = \beta + \phi$.

To determine the main-lobe footprint corresponding to a specified constant value $\hat{P}_s$ of normalized power density, we find the smallest (i.e., main-lobe) root α_s of the equation

$$\hat{P}(\alpha, \omega - \beta) = \hat{P}_s \tag{4-26}$$

for each ω-value in a suitable representative set spanning the interval $(0,2\pi)$. We assume, of course, that the satellite longitude λ_s and aim point coordinates ϕ_A, λ_A are given, as are the wavelength λ, the inclination β of the aperture's major axis, the lengths a, b of the aperture axes, and the aperture illumination functions X(x) and Y(y). If X(x) and Y(y) are even functions of their respective arguments, so that the illumination function f(x,y) is symmetric about both major and minor axes of the aperture, then the number of calculations per footprint can be reduced appreciably by choosing ω-values so as to exploit the resulting symmetry in $\hat{P}$ (or $\hat{F}$) whereby

$$\hat{P}(\alpha,\phi) = \hat{P}(\alpha, \pi - \phi) = \hat{P}(\alpha, \pi + \phi) = \hat{P}(\alpha, 2\pi - \phi) \quad . \tag{4-27}$$

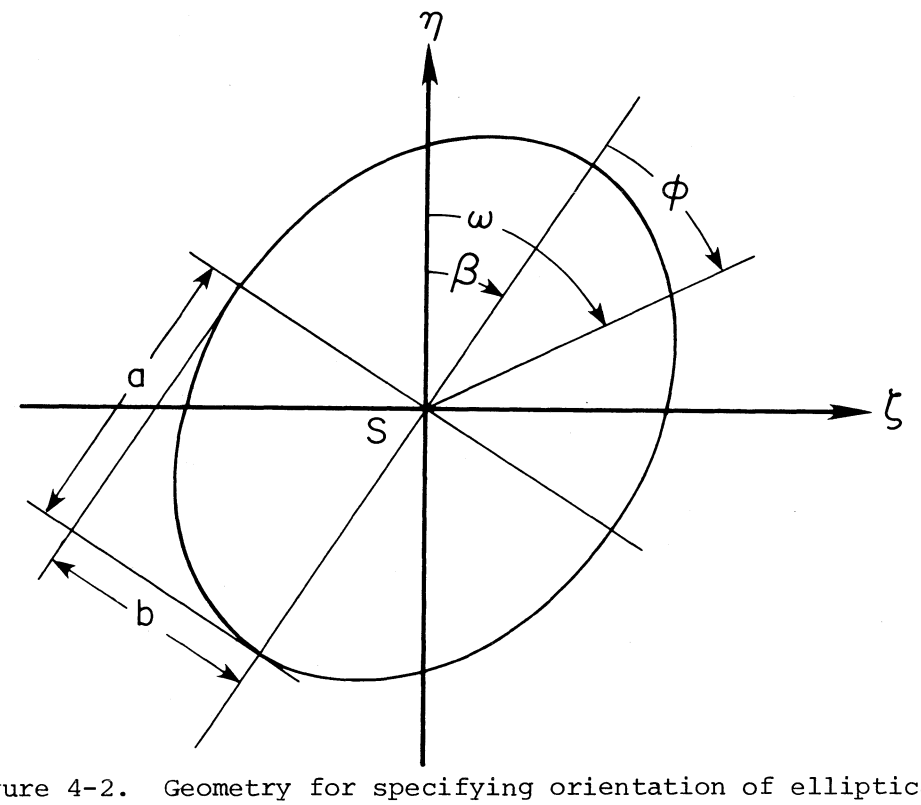

Figure 4-2. Geometry for specifying orientation of elliptical aperture antennas.

Thus, in such situations, one needs to actually calculate α-values only for a set of ω-values spanning an interval of length $\pi/4$. When ω is specified, the numerical procedures for obtaining α_s are essentially the same as those already outlined for the idealized circular aperture antenna.

5. RECTANGULAR APERTURE ANTENNAS

5.1 Introduction

When the elliptical aperture of the idealized antenna model described in section 4.1 is replaced by one that is rectangular, the resulting model can be used to simulate the main lobe of far-field patterns of such practical HF transmitting antennas as rectangular horns and certain cylindrical reflectors. Relevant geometry is indicated in Figure 5-1; except for the aperture, it is the same as that in Figure 4-1. Note that the aperture is centered (as before) at the origin of our right-handed system of coordinates (x,y,z) and consists of the rectangular region $|x| < a$, $|y| < b$ in the $z = 0$ plane. We assume that $a \gg \lambda'$ and $b \gg \lambda'$ (i.e., that the aperture is large, both of its dimensions encompassing several to many wavelengths); again, for later convenience in specifying the antenna's orientation, we require that $a \geq b$. We make the same assumptions about the aperture field as were made in the elliptical case--the field is linearly polarized, has a uniform phase, and a separable amplitude distribution $f(x,y)$ of the form (4-2).

5.2 Radiation Patterns

On assuming that the illumination distribution $f(x,y)$ vanishes outside the aperture (equivalent in this case to the conditions $X(x) = 0$ for $|x| > a$ and $Y(y) = 0$ for $|y| > b$), and neglecting edge effects, the normalized far-field amplitude pattern for the idealized rectangular aperture antenna may be approximated by

$$|\hat{F}(\theta,\phi)| = |F(\theta,\phi)/F(0,\phi)| \quad ,$$

where $F(\theta,\phi)$ is given by (4-7) and related formulas, just as in the case of the elliptical aperture. It is understood, of course, that in the present instance the integration is to be extended over the surface of the rectangular aperture. We may now write $F(\theta,\phi)$ as the iterated integral

$$F(\theta,\phi) = \int_{x=-a}^{+a} X(x) \exp(ik_x x) \left\{ \int_{y=-b}^{+b} Y(y) \exp(ik_y y)\, dy \right\} dx \quad , \tag{5-1}$$

which in turn may be written as a product of integrals

$$F(\theta,\phi) = \left(\int_{-a}^{+a} X(x) \exp(ik_x x)\, dx \right) \left(\int_{-b}^{+b} Y(y) \exp(ik_y y)\, dy \right) \quad . \tag{5-2}$$

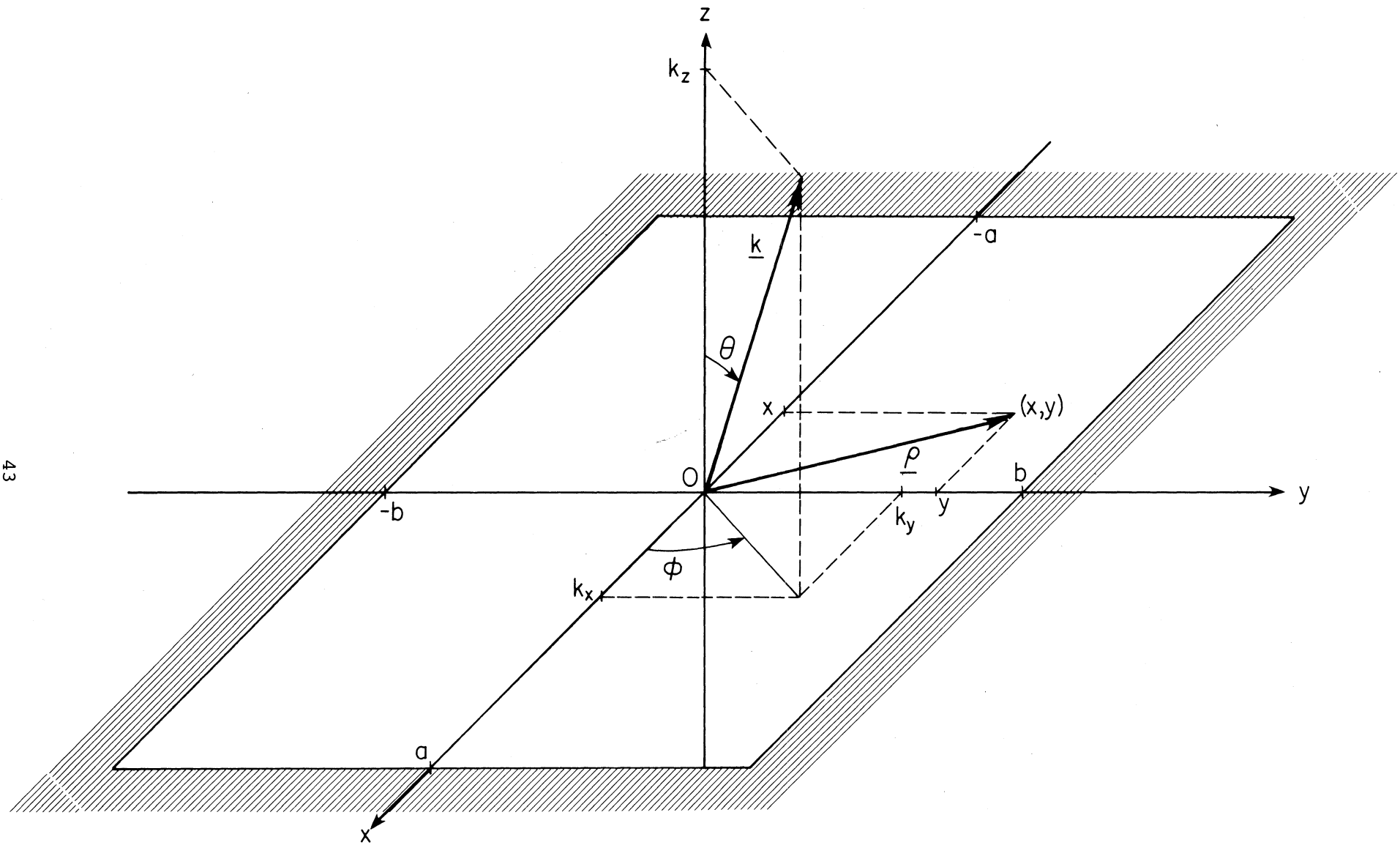

Figure 5-1. Geometry for the rectangular aperture antenna.

5.3 Some Special Cases

When a rectangular horn antenna is fed by a rectangular wave guide carrying a TE_{10} mode, the electric field in the horn aperture is quite uniform along the direction of the E-plane, but tapers to zero at the aperture edges along the direction of the H-plane (Kraus, 1950, p. 372). Provided that the horn flare angles are not too large, the main beam of such an antenna may be more or less crudely simulated by choosing

$$X(x) = 1 \tag{5-3a}$$

and

$$Y(y) = \cos\left(\frac{\pi y}{2b}\right) \quad . \tag{5-3b}$$

When these are substituted into (5-2), the resulting integrals are standard forms which, after a certain amount of manipulation, may be reduced to

$$\int_{-a}^{+a} \exp(ik_x x)\, dx = \frac{2}{k_x} \sin(k_x a) \tag{5-4}$$

and

$$\int_{-b}^{+b} \exp(ik_y y) \cos\left(\frac{\pi y}{2b}\right) dy = \frac{\pi b}{\frac{\pi^2}{4} - (k_y b)^2} \cos(k_y b) \quad , \tag{5-5}$$

where k_x, k_y are given by (4-6a) and (4-6b), respectively. Hence, for this model of the rectangular horn antenna,

$$F(\theta,\phi) = \frac{2\pi ab}{(k_x a)\left[\frac{\pi^2}{4} - (k_y b)^2\right]} \sin(k_x a) \cos(k_y b) \quad ; \tag{5-6}$$

we then find that

$$F(0,\phi) = \left(\frac{8}{\pi}\right) ab \quad , \tag{5-7}$$

so the normalized far-field pattern becomes

$$\hat{F}(\theta,\phi) = \frac{\pi^2}{4(k_x a)\left[\frac{\pi^2}{4} - (k_y b)^2\right]} \sin(k_x a) \cos(k_y b) \quad . \tag{5-8}$$

If we let $A = 2a/\lambda$ and $B = 2b/\lambda$ denote the aperture dimensions expressed in wavelengths, then (5-8) may be written in the form

$$\hat{F}(\theta,\phi) = \frac{1}{\pi h_A (1 - 4\, h_b^{\,2})} \sin(\pi h_A) \cos(\pi h_b) \quad , \tag{5-9}$$

where

$$h_A = A \sin\theta \cos\phi \tag{5-10a}$$

and

$$h_B = B \sin\theta \sin\phi \tag{5-10b}$$

Since we assumed at the outset that $a \geq b$, what we have just done is to model the situation where the E-plane is parallel to the long axis of the rectangular aperture. To get the pattern for the contrary case, where the E-plane is parallel to the short axis of the aperture, we need to choose

$$X(x) = \cos\left(\frac{\pi x}{2a}\right) \tag{5-11a}$$

and

$$Y(y) = 1 \quad . \tag{5-11b}$$

The resulting pattern can be written down by inspection; simply interchange A and B in (5-9) to get

$$\hat{F}(\theta,\phi) = \frac{1}{\pi h_B (1 - 4h_A^{\,2})} \sin(\pi h_B) \cos(\pi h_A) \quad . \tag{5-12}$$

Another useful representation of the aperture illumination amplitude for an idealized rectangular antenna consists of the product of the "raised cosine" functions given by (4-23a) and (4-23b). Because it includes the user-specified illumination tapers T_a and T_b (the physical significance of these parameters is pointed out in the discussion following (4-23b)), this model of the rectangular aperture antenna is more widely applicable than that described at the beginning of this section. The "raised cosine" model is also the one used by program FOOTPRINTS to simulate rectangular aperture antennas.

Note that (4-23a) and (4-23b) also can be used to simulate a rectangular horn antenna fed by a TE_{10} waveguide mode. When the E-plane is parallel to the long axis of the aperture, choose $T_a = 1$ and $T_b = 0$; on the other hand, when the E-plane

is parallel to the short axis of the aperture, one should choose $T_a = 0$ and $T_b = 1$. One ought to expect this model of a rectangular horn to be even cruder than the one considered earlier, where a somewhat more realistic distribution of aperture illumination was used.

When (4-23a) and (4-23b) are substituted into (5-2), the resulting integrals are again linear combinations of standard froms. After some manipulation, we find that

$$\int_{-a}^{+a} X(x)\ \exp(ik_x x)\ dx = a(1 + T_a) \left[1 + \frac{1-T_a}{1+T_a} \frac{(k_x a)^2}{\pi^2 - (k_x a)^2} \right] \frac{\sin(k_x a)}{k_x a} \quad ; \qquad (5\text{-}13a)$$

the analogous result for Y(y), obtained by inspection (replace x and a by y and b, respectively), is

$$\int_{-b}^{+b} Y(y)\ \exp(ik_y y)\ dy = b(1 + T_b) \left[1 + \frac{1-T_b}{1+T_b} \frac{(k_y b)^2}{\pi^2 - (k_y b)^2} \right] \frac{\sin(k_y b)}{k_y b} \quad . \qquad (5\text{-}13b)$$

When (5-13a) and (5-13b) are substituted into (5-2), we get

$$F(\theta,\phi) = ab(1 + T_a)(1 + T_b) \left[1 + \frac{1-T_a}{1+T_a} \frac{(k_x a)^2}{\pi^2 - (k_x a)^2} \right]$$
$$\times \left[1 + \frac{1-T_b}{1+T_b} \frac{(k_y b)^2}{\pi^2 - (k_y b)^2} \right] \frac{\sin(k_x a)}{k_x a} \frac{\sin(k_y b)}{k_y b} \quad , \qquad (5\text{-}14)$$

from which we see that

$$F(0,\phi) = ab(1+T_a)(1+T_b) \quad . \qquad (5\text{-}15)$$

Hence, the normalized far-field pattern for the rectangular aperture antenna with "raised cosine" illumination is $|\hat{F}(\theta,\phi)|$, where

$$\hat{F}(\theta,\phi) = \left[1 + \frac{1-T_a}{1+T_a} \frac{(k_x a)^2}{\pi^2 - (k_x a)^2} \right] \left[1 + \frac{1-T_b}{1+T_b} \frac{(k_y b)^2}{\pi^2 - (k_y b)^2} \right] \frac{\sin(k_x a)}{k_x a} \frac{\sin(k_y b)}{k_y b} \quad . \qquad (5\text{-}16)$$

An alternative form of (5-16), in terms of the aperture dimensions A and B introduced earlier, is

$$\hat{F}(\theta,\phi) = \left[1 + \frac{1-T_a}{1+T_a} \frac{h_A^2}{1-h_A^2} \right] \left[1 + \frac{1-T_b}{1+T_b} \frac{h_B^2}{1-h_B^2} \right] \frac{\sin(\pi h_A)}{\pi h_A} \frac{\sin(\pi h_B)}{\pi h_B} \quad . \qquad (5\text{-}17)$$

where h_A and h_B are given by (5-10a) and (5-10b), respectively.

5.4 Footprint Calculations for Rectangular Aperture Antennas

The geometry used to describe rectangular aperture antenna patterns is fitted into that used in section 2 to describe the antenna/satellite/earth configuration in the following way. First, the positive z-axis of Figure 5-1 is identified with the positive ξ-axis of Figure 2-1, so that the antenna's main-beam axis is directed toward the aim point A. The orientation of the rectangular aperture about the main-beam axis is then specified in a manner identical to that used earlier for the elliptical aperture antenna. Thus, as indicated in Figure 5-2, one prescribes the angle β from the positive η-axis to the long axis of the aperture (i.e., the $\phi = 0$ or positive x-axis of Figure 5-1). The angles α, ω in section 2 are then related to the angles θ, ϕ in Figure 5-1 by $\alpha = \theta$ and $\omega = \beta + \phi$.

To determine the main-lobe footprint corresponding to a specified constant value $\hat{P}_s$ of normalized power density, we need to find the smallest (i.e., main-lobe) root α_s of (4-26) for each ω-value in a suitable representative set spanning the interval $(0, 2\pi)$. The remarks concerning the solution of (4-26) for the elliptical aperture apply as well to the rectangular aperture and will not be repeated here.

For the special cases of aperture illumination considered in section 5.3, it is not necessary to execute a search procedure in order to isolate α_s in an interval (α_L, α_R). Instead, when $\phi = \omega - \beta$ is specified, one can calculate the smallest positive zero α_0 of $\hat{P}(\alpha,\phi)$ (or of $\hat{F}(\alpha,\phi)$), then set $\alpha_L = 0$ and $\alpha_R = \alpha_0$. For example, if one is using (5-9) to simulate the main beam of a rectangular horn, we see that $\hat{F}(\alpha,\phi) = 0$ when $|h_A| = 1, 2, \ldots$ and when $|h_B| = 3/2, 5/2, \ldots$. (Note that $|h_B| = 1/2$ does not correspond to $\hat{F}(\alpha,\phi) = 0$, since $\lim_{|h_B| \to \frac{1}{2}} \left[\cos(\pi h_B)/(1 - 4h_B^2)\right] = 1/4$.) In particular, if

$$\mu = \text{Max}\ \{A|\cos\phi|,\ \frac{2}{3} B|\sin\phi|\} \tag{5-18}$$

exceeds unity, then

$$\alpha_0 = \sin^{-1}\left(\frac{1}{\mu}\right) \quad . \tag{5-19}$$

A sufficient condition that $\mu > 1$ for all ϕ is that $A > \sqrt{2}$ and $B > \frac{3}{2}\sqrt{2}$; this will be satisfied for large apertures. The corresponding result for (5-12) is

$$\alpha_0 = \sin^{-1}\left(\frac{1}{\text{Max}\{B|\cos\phi|,\ \frac{2}{3} A|\sin\phi|\}}\right) \quad , \tag{5-20}$$

subject, of course, to the requirement that the indicated maximum exceeds unity.

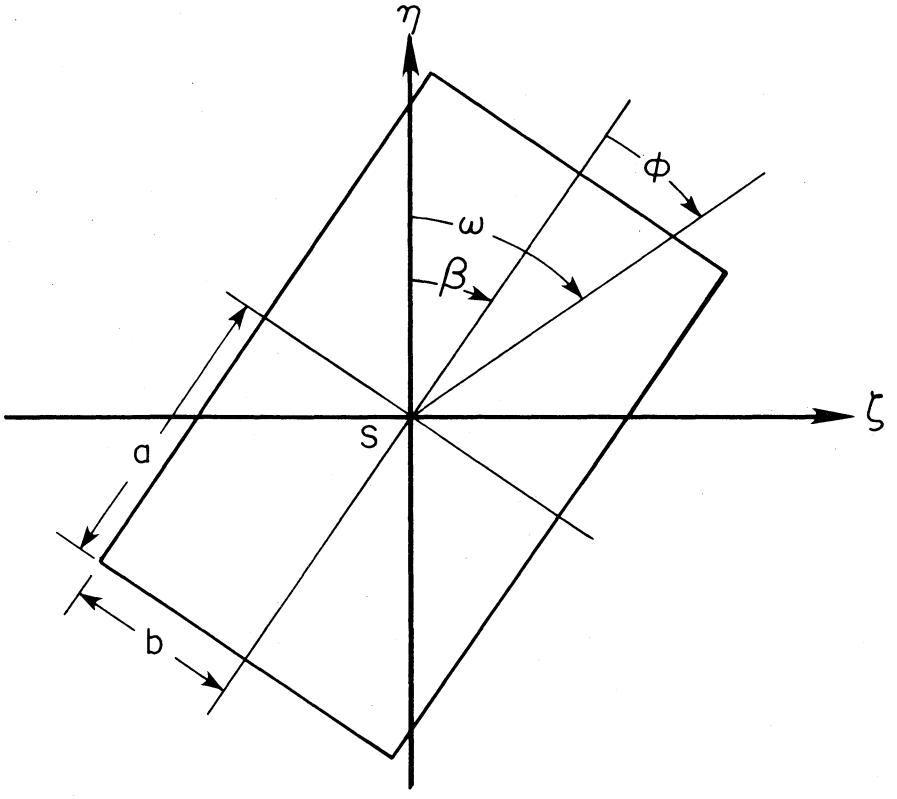

Figure 5-2. Geometry for specifying orientation of rectangular aperture antenna.

Table 5-1. Formulas for Evaluating μ in $\alpha_0 = \sin^{-1}(1/\mu)$, the First Null in Far-field Pattern of an Idealized Rectangular Aperture Antenna with "Raised Cosine" Illumination

	$0 \le T_a \le \frac{1}{7}$	$\frac{1}{7} \le T_a < 1$	$T_a = 1$
$0 \le T_b \le \frac{1}{7}$	$\mu = \mathrm{Max}\{\frac{1}{2} A\lvert\cos\phi\rvert, \frac{1}{2} B\lvert\sin\phi\rvert\}$	$\mu = \mathrm{Max}\left\{\left(\frac{2T_a}{1+T_a}\right)^{\frac{1}{2}} A\lvert\cos\phi\rvert, \frac{1}{2} B\lvert\sin\phi\rvert\right\}$	$\mu = \mathrm{Max}\{A\lvert\cos\phi\rvert, \frac{1}{2} B\lvert\sin\phi\rvert\}$
$\frac{1}{7} \le T_b < 1$	$\mu = \mathrm{Max}\left\{\frac{1}{2} A\lvert\cos\phi\rvert, \left(\frac{2T_b}{1+T_b}\right)^{\frac{1}{2}} B\lvert\sin\phi\rvert\right\}$	$\mu = \mathrm{Max}\left\{\left(\frac{2T_a}{1+T_a}\right)^{\frac{1}{2}} A\lvert\cos\phi\rvert, \left(\frac{2T_b}{1+T_b}\right)^{\frac{1}{2}} B\lvert\sin\phi\rvert\right\}$	$\mu = \mathrm{Max}\left\{A\lvert\cos\phi\rvert, \left(\frac{2T_b}{1+T_b}\right)^{\frac{1}{2}} B\lvert\sin\phi\rvert\right\}$
$T_b = 1$	$\mu = \mathrm{Max}\{\frac{1}{2} A\lvert\cos\phi\rvert, B\lvert\sin\phi\rvert\}$	$\mu = \mathrm{Max}\left\{\left(\frac{2T_a}{1+T_a}\right)^{\frac{1}{2}} A\lvert\cos\phi\rvert, B\lvert\sin\phi\rvert\right\}$	$\mu = \mathrm{Max}\{A\lvert\cos\phi\rvert, B\lvert\sin\phi\rvert\}$

A similar analysis can be carried out for the pattern (5-17) resulting from the "raised cosine" aperture illumination, but the details are more involved, since the values of T_a and T_b (as well as those of $A|\cos\phi|$ and $B|\sin\phi|$) influence the outcome. The results are summarized in Table 5-1.

Once α_s has been isolated in the interval $(0, \alpha_0)$, one can proceed as described in section 3.3, by successively applying the bisection method or the modified false position method to arrive at an estimate of α_s.

6. HELICAL BEAM ANTENNAS

6.1 Introduction

When antennas have the form of a (finite) circular helix that radiates in the so-called axial mode (Kraus, 1950), the far field has a well-defined main beam whose maximum is in the direction of the helix axis. Such antennas are known as helical beam antennas and can be made sufficiently directional that they may, under certain circumstances, be suitable for use on satellites.

A fairly detailed discussion of the characteristics of helical antennas is given in the standard text by Kraus (1950, ch. 7); here we simply mention a few salient features of the helical beam antenna. First, for a helix to radiate in the axial mode, the helix circumference C must roughly equal the (free space) wavelength of the operating frequency; in particular, C (when expressed in wavelengths) should lie in or near the range 3/4 - 4/3. At the same time, the pitch angle of the axial mode helix should lie in or near the range 10° - 20°, the optimum angle being 12° - 15°; the spacing S between turns (expressed in wavelengths) should lie in or near the range 0.1 - 0.5. Finally, the number n_t of turns in a helical beam antenna should exceed about 3 (for satellite applications, n_t will usually be at least several times this value).

6.2 Radiation Patterns

As indicated in Figure 6-1, an n_t-turn circular helix antenna is centered at the origin of a right-handed system of rectangular coordinates (x,y,z) so that the helical axis lies along the z-axis. If one represents the pattern of a single turn by $\cos\theta$ (where, as shown in Figure 6-1, θ is the angle from the helix axis to the direction of the observer) and assumes what Kraus (1950, p. 190) calls the "increased directivity condition" to hold, then the main lobe of the antenna's normalized far-field pattern can be approximated by $|\hat{F}(\theta)|$, where (Kraus, 1950, p. 202)

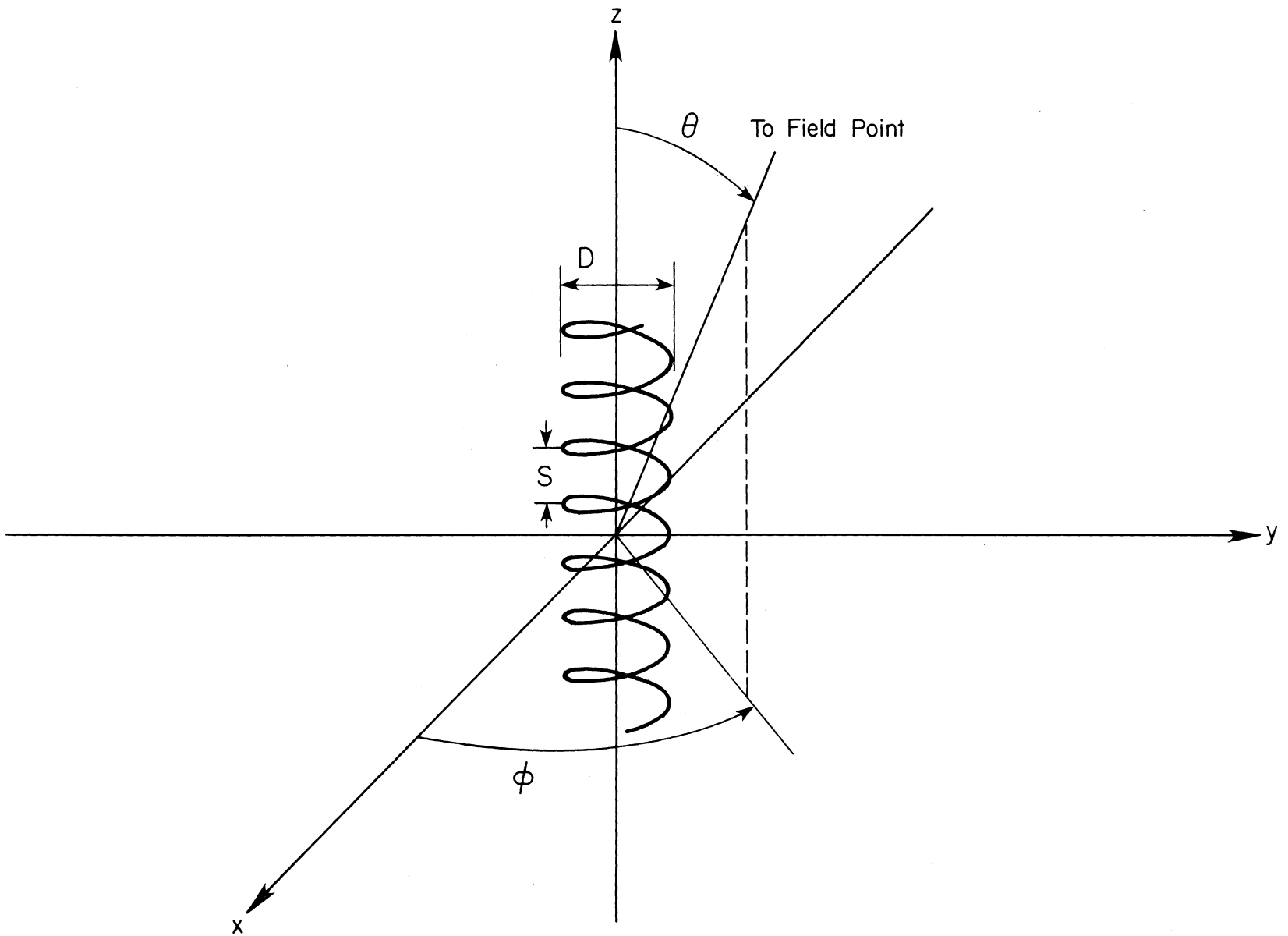

Figure 6-1. Geometry for the helical beam antenna.

$$\hat{F}(\theta) = \sin\left(\frac{\pi}{2n_t}\right) \frac{\sin(n_t\ \psi/2)}{\sin(\psi/2)} \cos\theta \quad , \tag{6-1}$$

$$\psi = 2\pi \left[S(1 - \cos\theta) + \frac{1}{2n_t} \right] \quad , \tag{6-2}$$

and (as previously noted) S is the spacing between turns (expressed in wavelengths).

Note that this pattern has circular symmetry about the helix axis. It also should be emphasized that the preceding expression for $|\hat{F}(\theta)|$ does not reliably represent the side-lobe pattern of an actual antenna.

6.3 Footprint Calculations for Helical Beam Antennas

To fit the helix geometry of the preceding section into the antenna/satellite/earth configuration described in section 2, we identify the (positive) z-axis of Figure 6-1 with the (positive) ξ-axis of Figure 2-1. The helical axis of the antenna is then directed at the aim point, and the angle θ in section 6.2 is identified with the angle α in section 2. Owing to the pattern's circular symmetry, the relation of the x and y axes of Figure 6-1 to the η and ζ axes of Figure 2-1 is immaterial.

Because the far-field pattern of our idealized helical beam antenna has circular symmetry, the procedure for calculating the main-lobe footprint corresponding to a prescribed constant value $\hat{P}_s$ of normalized power density is, in principle, exactly the same as that used for the idealized circular aperture antenna, with the exception of one important simplifying feature. This simplification consists of not having to execute a search procedure in order to isolate the desired (main-lobe) root α_s of

$$\hat{F}(\alpha) = \hat{P}_s^{\ 1/2}$$

in an interval (α_L, α_R). Instead, one can easily calculate the smallest (positive) zero α_0 of $\hat{F}(a)$, then set $\alpha_L = 0$ and $\alpha_R = \alpha_0$. One then preceeds as described in section 3.3, by successively applying the bisection method or the modified false position method to arrive at an estimate of α_s.

From (6-1), and (6-2), we see that $\hat{F}(\alpha_0) = 0$ implies that $n_t\ \psi/2 = \pi$, or

$$2\pi\ S(1 - \cos\alpha_0) + \frac{1}{2n_t} = \frac{2\pi}{n_t} \quad . \tag{6-3}$$

From this, it follows that

$$\cos\alpha_0 = 1 - \frac{1}{2n_t S} \tag{6-4}$$

and

$$\alpha_0 = \mathrm{Tan}^{-1}\left[\frac{(4n_t S - 1)^{1/2}}{2n_t S - 1}\right]$$

7. REFERENCES

Abramowitz, M., and I.A. Stegun, eds. (1964), Handbook of Mathematical Functions, Nat. Bur, Stds. Appl. Math. Ser. 55 (U.S. Government Printing Office, Washington, DC).

Adams, R.J., and K.S. Kelleher (1950), Pattern calculations for antennas of elliptical aperture, Proc. IRE 38, No. 9 September, p. 1052.

Collin, R.E. (1969), Radiation from apertures, ch. 3 in Antenna Theory, Part 1, ed. R.E. Collin and F.J. Zucker (McGraw-Hill Book Company, Inc., New York, NY), pp. 61-92.

Conte, S.D., and C. deBoor (1965), Elementary Numerical Analysis: An Algorithmic Approach, Second edition (McGraw-Hill Book Company, Inc., New York, NY), pp. 31-32.

Gary, A., G.B. Mathews, and T.M. MacRobert (1922), A Treatise on Bessel Functions and Their Applicatons to Physics (MacMillan and Co., Ltd., London), p. 62.

Haakinson, E.J., D.E. Skinner, K.P. Spies, and G.J. Bridgewater (1977), Automated computing and plotting of geostationary satellite earth footprints: program FOOTPRINTS users manual, OT Report 77-120 (U.S. Dept. Commerce, Office of Telecommunications.

Hamming, R.W. (1971), Introduction to Applied Numerical Analysis (McGraw-Hill Book Company, Inc., New York, NY), pp. 47-48.

Kraus, J.D. (1950), Antennas (McGraw-Hill Book Company, Inc., New York, NY).

Ott, R.H. (1975), A numerical method for generating earth coverage footprints from geostationary antennas, U.S. Postal Service Rept. (NTIS Access. No. PB252688).

Sciambi, A.F. (1965), The effect of the aperture illumination on the circular aperture antenna pattern characteristics, Microwave 8, No. 8, August, pp. 79-84.

Silver, S. (1949), Aperture illumination and antenna patterns, ch. 6 in Microwave Antenna Theory and Design, ed. S. Silver, M.I.T. Rad. Lab. Ser., vol. 12 (McGraw-Hill Book Company, Inc., New York, NY), pp. 169-199.

Watson, G.N. (1944), A Treatise on the Theory of Bessel Functions, second edition (Cambridge University Press, London).

Wheelon, A.D. (1968), Tables of Summable Series and Integrals Involving Bessel Functions (Holden-Day, San Francisco, CA).

FORM **NTIA-29**
(4-80)

U.S. DEPARTMENT OF COMMERCE
NAT'L. TELECOMMUNICATIONS AND INFORMATION ADMINISTRATION

BIBLIOGRAPHIC DATA SHEET

1. PUBLICATION NO. NTIA Report 80-51	2. Gov't Accession No.	3. Recipient's Accession No.

4. TITLE AND SUBTITLE
CALCULATION OF GEOSTATIONARY SATTELLITE FOOTPRINTS FOR CERTAIN IDEALIZED ANTENNAS

5. Publication Date
October 1980

6. Performing Organization Code
NTIA/ITS-1

7. AUTHOR(S)
K.P. Spies and E.J. Haakinson

8. PERFORMING ORGANIZATION NAME AND ADDRESS
National Telecommunications and Information Admin.
Institute for Telecommunication Sciences
Boulder, CO 80303

9. Project/Task/Work Unit No.

10. Contract/Grant No.

11. Sponsoring Organization Name and Address
Office of Telecommunications
Spectrum Analysis Group

12. Type of Report and Period Covered
NTIA Tech. Report

13.

14. SUPPLEMENTARY NOTES

15. ABSTRACT *(A 200-word or less factual summary of most significant information. If document includes a significant bibliography or literature survey, mention it here.)*

This report describes methods for calculating, under certain simplifying assumptions, footprints (contours of constant power density) for idealized models of several common types of transmitting antennas (circular aperture, elliptical aperture, rectangular aperture, and helical beam antennas), and for antenna beams of specified but rather arbitrary shape. The transmitter is mounted on a satellite at a prescribed location in the geostationary orbit and has its main-lobe axis directed toward a given aim point on the earth.

(Continued on back)

16. Key Words *(Alphabetical order, separated by semicolons)*
Antenna patterns; footprints; geostationary satellite; power density contours

17. AVAILABILITY STATEMENT ☒ UNLIMITED. ☐ FOR OFFICIAL DISTRIBUTION.	18. Security Class. *(This report)* Unclassified 19. Security Class. *(This page)* Unclassified	20. Number of pages 56 21. Price:

15. Abstract (continued).

Formulas are first derived for calculating the intersection of the earth with a ray emanating from a given geostationary satellite and having a prescribed direction in space. For each idealized antenna type, procedures are next discussed for finding those directions in space where the relative power density has a specified constant value; intersection formulas are then applied to locate the corresponding footprint. Far-field patterns are approximated for aperture antennas by evaluating Fourier transforms of assumed aperture illumination distributions, and for the helix by assuming it radiates in the axial mode. Owing to gross discrepancies between actual and ideal side-lobe patterns, the analysis is confined to the main lobe of idealized antenna models.

☆ U.S. GOVERNMENT PRINTING OFFICE: 1980—777-927/150 Region No. 8